A SURVEY OF RADIATION EFFECTS ON TRAPATT AND LSA DEVICES

by

VERNON WILLIAM BRATTON, JR., B.S. in E.E.

A THESIS

IN

ELECTRICAL ENGINEERING

Submitted to the Graduate Faculty
of Texas Tech University in
Partial Fulfillment of
the Requirements for
the Degree of

MASTER OF SCIENCE

IN

ELECTRICAL ENGINEERING

Approved

May, 1973

ACKNOWLEDGEMENTS

I am deeply grateful to Dr. D. K. Ferry for his patience and guidance during the preparation of this thesis. I am also indebted to Dr. H. F. Martz, Jr. and Dr. J. D. Reichert for their advice and helpful criticism.

TABLE OF CONTENTS

LIST OF TABLES

LIST OF FIGURES

CHAPTER I

INTRODUCTION

Military systems have always been required to operate under many different environmental conditions. From the advent of the nuclear age additional requirements have been imposed on the designers of military hardware to insure battle survival. Many of these systems now are composed of complex electronic equipment which must function during and after exposure to nuclear radiation in the vicinity of a nuclear detonation. The methods used and the extent to which the military electronics are hardened depends on whether the system will be operated in an exo-atmospheric* or an endo-atmospheric environment and upon the maximum weapon yield expected.

In the endo-atmospheric nuclear environment the system designer is concerned with aircraft, early boost phase and terminal reentry phase of Inter-Continental Ballistic Missiles (ICBM), tactical air-to-air and surface-to-air missiles and surface systems.[1] In this environment the nuclear weapons used can be both tactical and strategic devices. The tactical weapons will more than likely be the fission type with yields in the range 1-20 kiloton with 1 kiloton approximately equivalent to 10^{12} calories.[2] The strategic weapons will probably be fusion type carried by ICBM's and consist of yields of 1 megaton or greater.[2] Nuclear effects upon systems in this environment are produced by prompt and delayed gamma rays, neutrons, thermal radiation,

---

*Exo-atmospheric environment is defined as that area of space which is above 100,000 feet in altitude.

blast and overpressure and electromagnetic pulses. It is assumed in this thesis that the blast and thermal radiation will not penetrate to the interior of the military system and affect the electronic equipment. The gamma ray and neutron total doses are rapidly reduced as the distance from the point of detonation increases.[1] The environmental contours for 1 megaton and 10 kiloton yield weapons, detonated at sea level, are shown in Figs. 1.1 and 1.2, respectively.

In the exo-atmospheric nuclear environment, the system designer is concerned with the effects of gamma rays, x-rays, neutrons and electromagnetic pulses (EMP) on satellites and the late boost, free-flight, and early reentry phases of ICBM's.[1] Since there is no atmosphere in this environment, the system designer is not concerned with blast and thermal radiation.[1] The environmental contours for a 1 megaton burst is shown in Fig. 1.3.

Solid-state devices are highly desirable for use in military electronics due to their small physical size and light weight. For this reason, numerous investigations have been conducted concerning radiation effects of solid-state material and devices.

A. Radiation Environment

The radiations of major concern to engineers are fast neutrons and gamma rays.[3,4] EMP is also of concern due to the large voltages and currents which can be induced in electronic systems.

Fast neutrons are those neutrons with energies greater than 10 keV. The unit used for describing the intensity of neutron radiation is flux and is generally defined as the number of particles flowing per unit time through an imaginary sphere of unit cross-sectional area

N - Neutron	10^{12} n/cm^2
G - Prompt Gamma	100 rads.
T - Thermal	10 cal/cm^2
P - Overpressure	1 psi

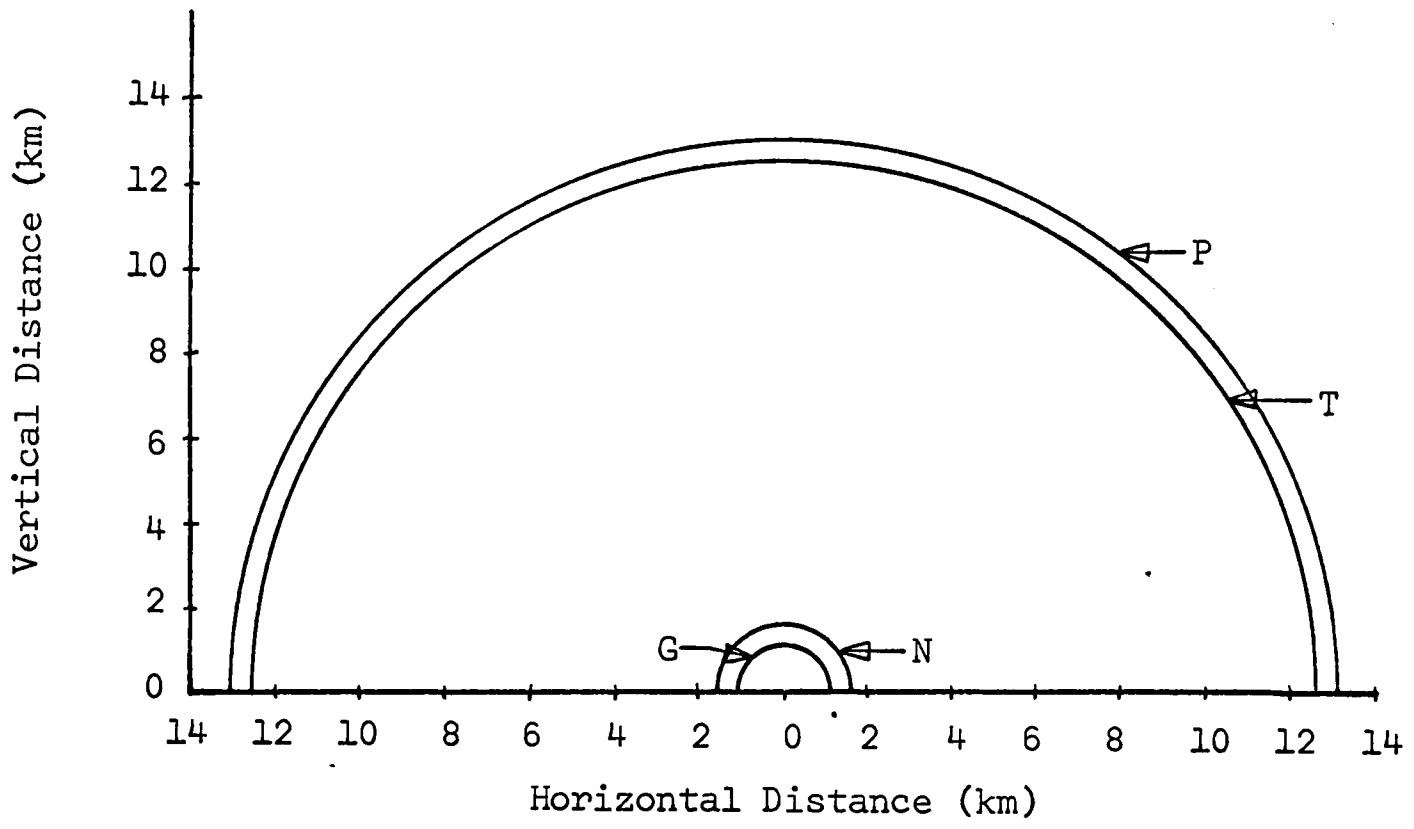

Figure 1.1. Environmental contours for a 1 megatron surface burst. (After Poll.[1])

N - Neutrons	10^{12} n/cm^2
G - Prompt Gamma	100 rads
T - Thermal	10 cal/cm^2
P - Overpressure	1 psi

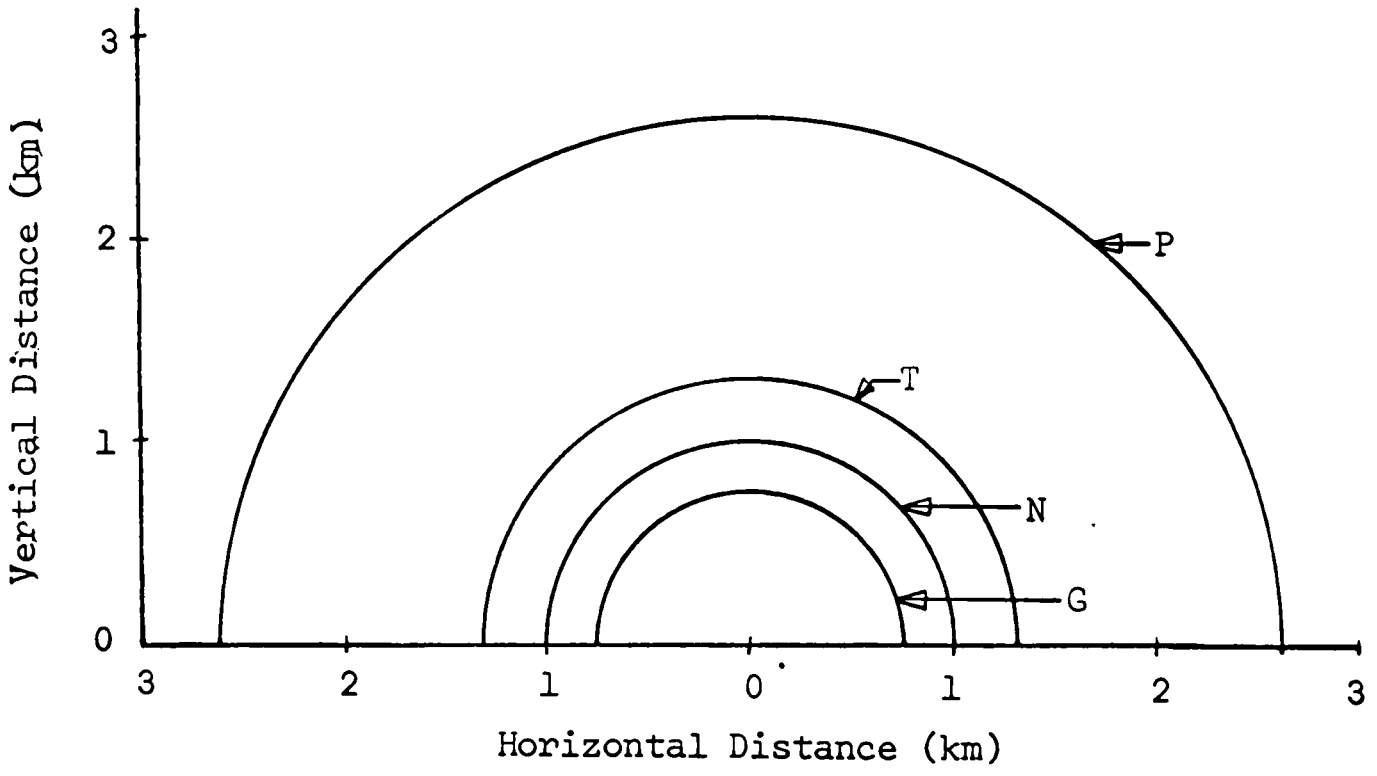

Figure 1.2. Environmental contours for a 10 kiloton surface burst. (After Poll.[1])

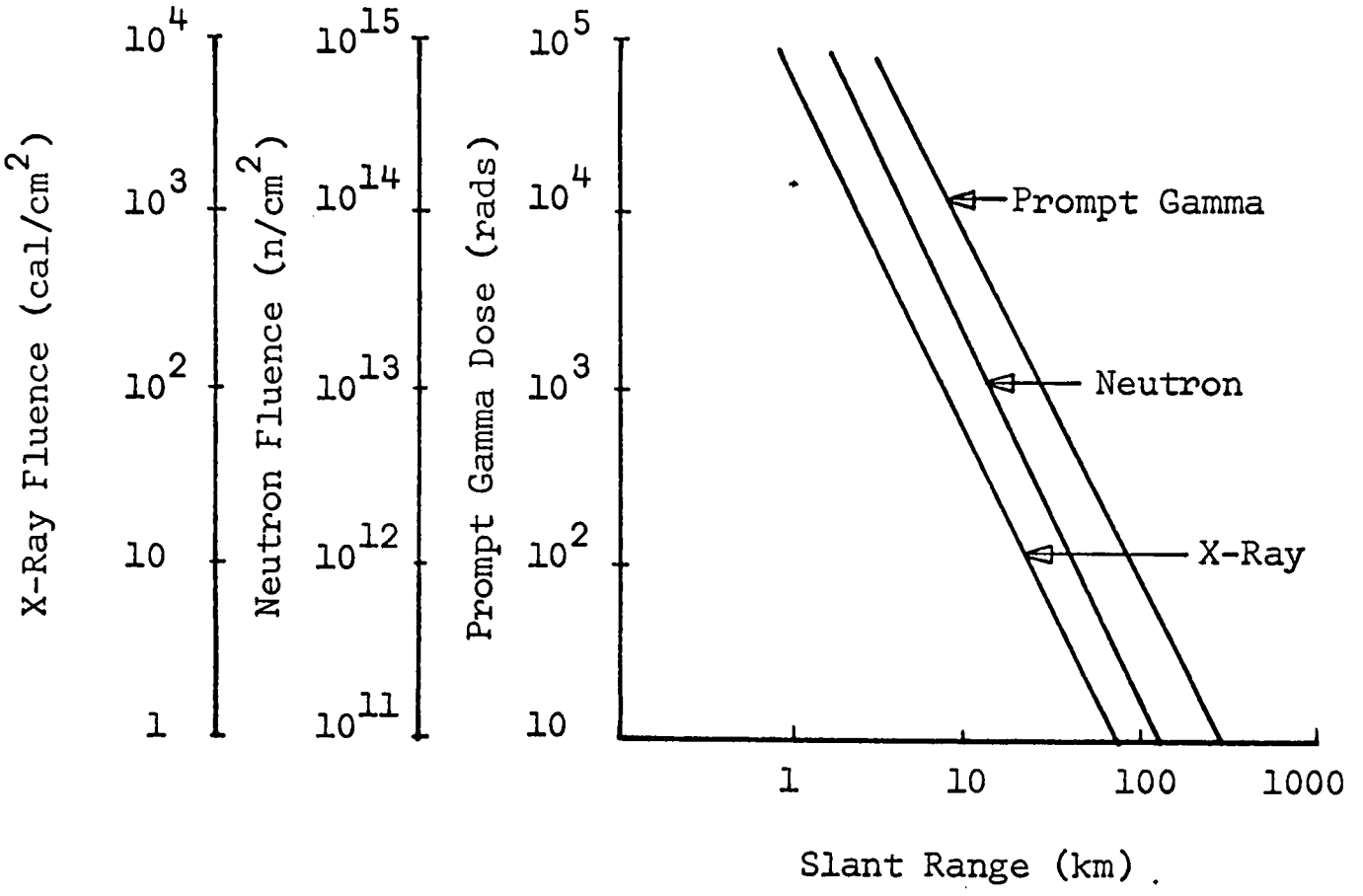

Figure 1.3. Environmental contours for an exo-atmospheric 1 megaton burst. (After Poll.[1])

(particles/cm^2-sec).[3,4] The unit used to describe neutron exposure is fluence which has the units particles/cm^2. Fluence is also called the time integral of the flux. Fast neutrons, colliding with solid-state material, produce displacement and ionization damage with the displacement effects being considered, usually, as the most serious degradation effect in devices.[4] Neutrons cause crystal atoms to be displaced from their normal position in the crystal lattice locations resulting in unoccupied lattice positions called vacancies. The displaced atom is called an interstitial atom and will come to rest in a position out of the lattice structure with the distance traveled depending on the energy of the incident neutron. If the recoiling atom has sufficient energy, clusters of secondary interstitial and vacancy defects will also be formed. Displacement damage in solid-state devices causes a reduction in the minority carrier lifetime and an increase in resistivity.[3,4] In addition to the displacement effects, neutrons can cause ionization effects either directly or indirectly but are usually neglected since the effects are normally small compared to the ionization produced by gamma rays.

The unit used for describing the exposure dose of gamma radiation is the roentgen and is the amount of radiation which causes a specified amount of ionization in air (87.7 ergs per gram).[3] The unit used for describing the absorbed dose is the rad which is the amount of radiation required to deposit 100 ergs/gm in a certain material.[5] The type of material must be defined when using the term rad; however, in studies of effects on semiconductors, silicon is usually used as the reference and will be used in this thesis except where noted otherwise.

Gamma rays emitted from a nuclear weapon burst travel at the speed of light and are called prompt gammas. The prompt gamma pulse is usually short compared with the device or circuit time constants.[5]

For most of the gamma rays of interest, the Compton process is the dominant energy-loss mechanism, particularly in low atomic number materials such as silicon.[5] In the Compton process, the gamma ray is scattered by a free electron, losing an appreciable fraction of its energy which, in turn, is acquired by the electron. The electron then deposits its energy by ionization. The scattered and degraded gamma ray is available for further Compton interaction.[5] As a result of these events, energy from the gamma rays is absorbed in the generation of heat and in the excitation of electrons. For most semiconductors, the latter is more important, although for high powered devices, the increase in heat alone may be enough to destroy the device. The excited electrons also produce electron-hole pairs which can result in transient damage effects to some semiconductors. Transient damage effects result from the generation of photocurrents due to the flow of minority carriers across the junction of a device.[4] These currents can be calculated from the physical characteristics of the device and the external voltages and impedances.

The EMP effect is present in both types of weapon environments and may induce large currents or voltages in electronic systems.[1] The induced electric field is a fast-rising pulse which may have a maximum amplitude as large as tens of thousands of volts per meter, at altitudes below approximately 100,000 feet. The field decreases at altitudes above 100,000 feet. Since EMP effects can occur at great

distances from a nuclear weapons detonation, an electronic system must be hardened against this effect even when neutron and gamma ray fluences are very low. EMP induced currents along air-frame surfaces and cable runs may couple energy into system electronics unless preventive measures are taken. Poll[1] indicated that EMP effects could be prevented by using good engineering practices for electromagnetic interference suppression. A single point grounding scheme must be used to avoid ground loops as well as good radio frequency suppression techniques. He further indicated that all cable runs must be shielded with no gaps left at connections, and that RF gaskets must be used on enclosures. EMP effects will not be discussed further in this thesis since damage to system electronics can be prevented by the techniques discussed above.

Solid-state microwave devices have been developed, within the past few years, to the extent that the use of high peak-power oscillators in some military systems is possible. The Limited Space-charge Accumulation (LSA) mode of the negative-resistance diodes and the Trapped Plasma Avalanche Triggered Transit (TRAPATT) mode of the avalanche diodes appear to be the most logical choice for high peak-power sources needed for use in beacons, transponders, and light-weight ranging radars. The heart of both the LSA and TRAPATT devices is the diode.

B. TRAPATT Device Operation

The TRAPATT oscillator is capable of operating between several hundred MHz to approximately ten GHz with efficiencies ranging up to 60 percent.[6] The high quality diodes are typically silicon p^+nn^+

structures with the n-type depletion region varying from approximately 0.1 to 0.5 mil. The high efficiency mode of oscillation was first reported in April, 1967, by Prager, Chang, and Weisbrod.[7] The operation was referred to as anomalous because the oscillation frequency was considerably less than that of the normal IMPATT (Impact Avalanche Transit-Time) mode, and the efficiency was larger than that for the IMPATT mode. Clorfeine, et al,[8] and others[9] have provided an analytic description of the TRAPATT mode utilizing a simplified physical model. In this model, the p^+ and n^+ contact regions are so heavily doped that their conductivity is considered infinite. The n-type region doping is low enough that the diode is well punched through into the n^+ region prior to breakdown. The ionization rates for electrons and holes are considered equal and constant above a critical field, E_a, and zero for values below E_a. The carrier velocities are considered equal and constant (approximately 10^7 cm/sec in silicon) above a saturation field, E_s, and proportional to the field ($v = \mu E$) below E_s.[9,10,11] With the diode biased such that the electric field at the p^+n junction has obtained a value just below E_a and with a step in the current J_o applied, J_o will drive the field up uniformly throughout the diode until E exceeds E_a. When E_a is exceeded, electron-hole pairs are created by impact ionization. If J_o is sufficiently large ($J_o > qv_sN_D$), an avalanche shock front (ASF) is formed and propagates through the diode toward the nn^+ junction at a velocity v_z greater than the saturated velocities v_s of the carriers leaving a dense electron-hole plasma in its wake.[8,11] Since the density of electrons in the immediate wake of the wave front is higher than the hole density,

the electron-rich region rapidly reduces the field to near zero. Since the internal field is well below the saturated value E_s, the carriers will be trapped for a long time before they are completely swept out. During the extraction period, the residual carriers diffuse out of the depletion region leaving a carrier deficient region near each boundary causing the field to rise.[8] When the critical field is reached, the entire process is repeated. As long as the current J_o is held constant, the device is not useful from a power generation standpoint. However, if the applied current is reduced to zero at the time the plasma is cleared and the field is slightly below avalanche, then the device voltage would be constant until a new current pulse is applied to the diode. Thus, the diode will efficiently convert DC power to RF power, and Clorfeine calculated theoretical efficiencies of 50 to 60 percent for a square wave of external current.

C. LSA Device Operation

The Limited Space-charge Accumulation (LSA) mode was observed by Copeland[12] in computer simulations of a bulk negative resistance device. The negative resistance appears in n-type gallium arsenide due to the two types of valleys in the conduction band. The negative resistance effect is due to the electrons in gallium arsenide exhibiting a negative differential mobility.[13] For a negative differential mobility the electron drift velocity increases with increasing electric field up to a certain point and then decreases. Indium phosphide and cadmium telluride are also known to exhibit a negative differential resistivity when biased above their individual threshold; however, gallium arsenide is the most widely studied. The negative mobility

mechanism in gallium arsenide is a direct result of the energy band structure of the material.[13] Most of the electrons are located in the lower conduction band (central) valley at room temperature for low electric fields.[13,14] These carriers have a low effective mass and a high mobility which makes it easy to accelerate to higher energies. Since the energy separation between the lower central valley and higher satellite valley is 0.36 eV for n-type gallium arsenide, electrons are easily scattered into the satellite valley, where they have much higher effective mass and much lower mobility.[13] This then is the basic mechanism involved in the operation of bulk n-type gallium arsenide oscillators.

The LSA oscillator is capable of operating between 1 and 300 GHz with efficiencies ranging up to 20 percent at low duty cycles.[6] The greatest efficiencies are obtained between 10 and 40 GHz. The high quality diodes consist of an epitaxially grown, n-type, gallium arsenide active layer, 2 to 8 mils in length, between two heavily doped n^+ layers.[6] Copeland explained the characteristics of the LSA mode as this:

1. The frequency of operation is higher than the reciprocal of the carrier transit time.
2. The frequency of oscillation is determined by the frequency of the circuit resonance.
3. The power output and efficiency are equal to or higher than when the same device is operated in the transit time frequency mode or in the quenched domain mode.

In order for good quality gallium arsenide diodes to operate in the LSA mode, Copeland[15] indicated that the doping to frequency (N_D/f)

ratio should be in the following range:

$$2 \times 10^4 < N_D/f < 2 \times 10^5 \text{ sec/cm}^2. \qquad (1.1)$$

The tuned circuit containing the diode must be properly loaded so that the voltage across the device swings below the threshold voltage for a short part of each cycle. Copeland[12] further indicated that the bias voltage should be more than twice the threshold voltage for Gunn oscillations in order that gallium arsenide diodes will function in the LSA mode. When the sample is oscillating in the LSA mode, the electric field across the diode rises from below the threshold value to a value more than twice the threshold field so quickly that the space-charge distribution associated with a high field domain does not have time to form. In this case there exists only an accumulation layer near the source contact, and the field over most of the device is in the negative resistance range.[12] The dielectric relaxation time, $\epsilon/(N_D|\bar{\mu}_n|e)$, when the electric field is below threshold must be short compared to the fraction of a period when the field in the diode is below threshold in order for the accumulation layer to disappear. If the frequency increases, the distance over which the accumulation layer travels decreases, and more electrons contribute energy to the load.[14] In this case, the efficiency in the LSA mode increases with frequency. The size of the diode is limited primarily by the wavelength in the material and the skin depth.[15] Typical device areas range from 100 to 500 square mils.[6]

Chapter II of this thesis is devoted to the effects of neutron radiation exposure to IMPATT, TRAPATT, LSA and Gunn devices. Chapter III contains a discussion on ionization effects, due to gamma

ray experimental data relating to the TRAPATT and LSA modes. General principles for extrapolating to these devices are discussed. Chapter IV contains the conclusions and comments on the radiation tolerance and hardening of the two high powered devices.

CHAPTER II

NEUTRON RADIATION EFFECTS

Fast neutron bombardment of materials such as silicon and gallium arsenide used in TRAPATT and LSA devices, respectively, results in the displacement of atoms from ordered positions in the crystal lattice. The extent of the damage effect is dependent upon the spectrum and fluence of the incident neutrons. The displacement of atoms from their normal position results in unoccupied lattice positions called vacancies. The primary recoiling atom, after being hit by the incident neutron, will come to rest in a position out of the lattice structure. This produces what is called an interstitial atom. When a displaced atom traverses through the lattice of a crystalline solid, the most important means of energy loss is through elastic collisions with atoms of the lattice. If a lattice atom receives an energy E_p in excess of E_d, where the latter is defined as the Wigner energy or displacement energy, it is displaced from its normal lattice site. The value of E_d is usually considerably larger than the energy required to form a vacancy-interstitial pair by a thermodynamically reversible process.[16] This is due to the recoil taking place before the neighboring atoms have the opportunity to relax to an equilibrium. For typical monatomic solids, E_d usually has a value between 10 and 30 eV, while the energy for the thermal generation of vacancy-interstitial pairs is between 3 and 6 eV.[16] For example, the displacement energy required for silicon is 13 eV. The bombarding neutron can make one or a number of primary collisions. The knock-on atom, the primary recoil or what is also

known as the primary, continues to produce more displacements (secondaries) on its own due to its interaction with other lattice atoms, and these displaced atoms may in turn produce what are known as tertiary displacements. This chain continues until the energy of each particle has been degraded to a level that E_d can not be transferred in subsequent collisions. This multiplying effect leads to the displacement cascades which account for the major portion of defects created by neutron bombardment. Each collision by fission neutrons whose average energies[16] are approximately 1.5 MeV produces an average of between 317 and 2500 displacements.[17] Neutrons create these displacements in small spherical regions called clusters. The vacancies resulting are mainly trapped in a highly disordered region of the cluster. A displacement cascade therefore consists of a disordered region with various lattice sites empty.

It has been shown,[18,19] that in many semiconductor materials, fast neutron irradiation results in defect clusters within which the defect density can be much greater than the material doping density. In silicon and gallium arsenide, the energy levels corresponding to these defects in the cluster lie deep in the energy gap.[20] Within these disordered regions, the material is essentially compensated intrinsic. Gassick[19] originally proposed a cluster model in which the deep defects within a disordered region become charged by trapping majority carriers from the surrounding undamaged material. The free carriers are thereby removed from the area surrounding the cluster which creates a depleted charge layer of opposite polarity to the cluster charge, as shown in Gregory's model[20,21] for n-type silicon in Fig. 2.1. R_1 is defined as

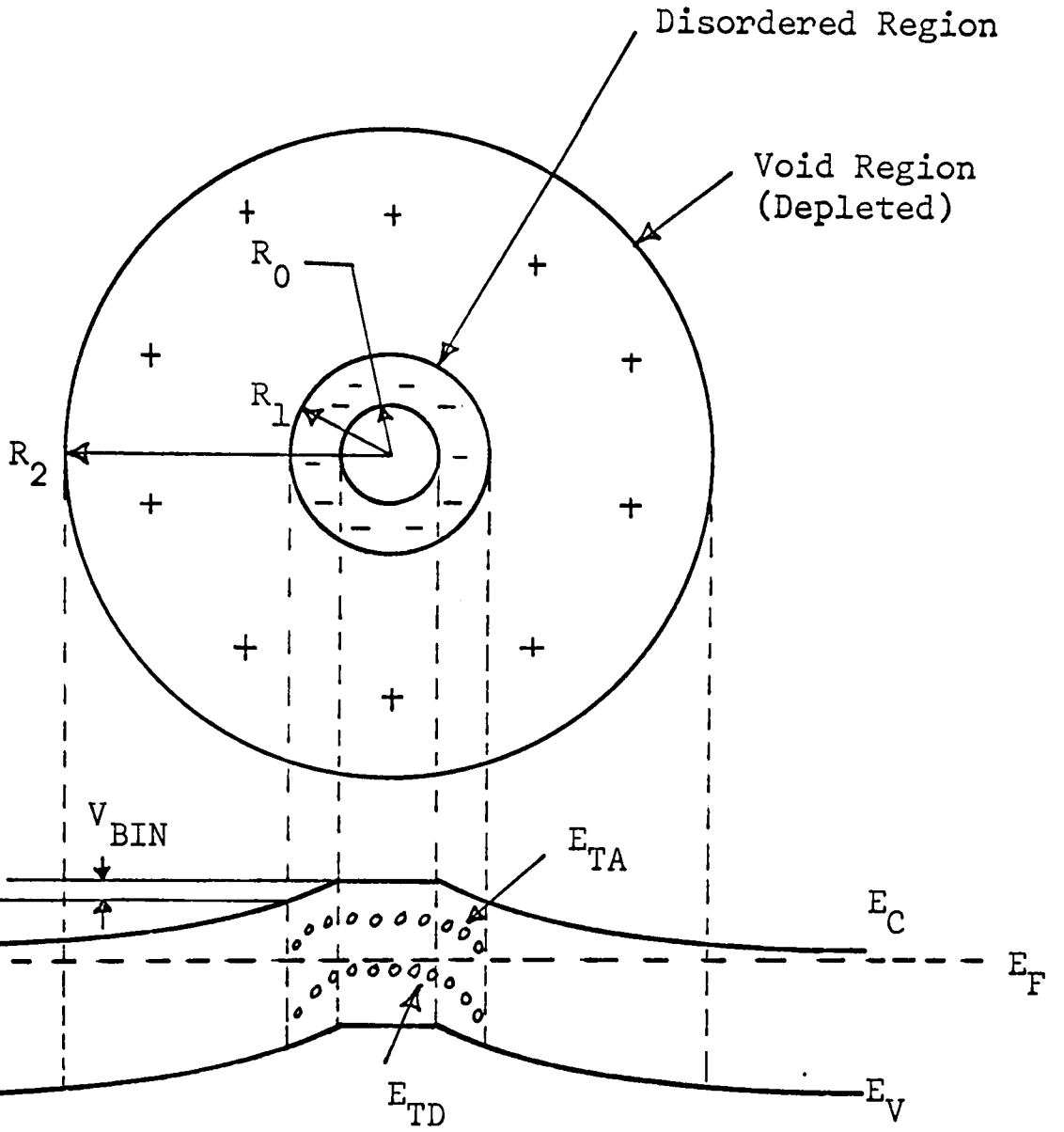

$$V_B = (qN_D R_1^2/3\epsilon)\left[\frac{1}{2} + (R_2/R_1)^3 - \frac{3}{2}(R_2/R_1)^2\right]$$

$$V_{BIN} = (qN_T R_1^2/6\epsilon)\left[1 - 3(R_0/R_1)^2 + 2(R_0/R_1)^3\right]$$

Figure 2.1. Schematic model for the neutron-produced cluster in n-type silicon. (After Gregory.[20,21])

the cluster radius, R_2 and R_o are the outer and inner boundaries of the space-charge region, respectively. E_{TA} and E_{TD} are the dominant acceptor and donor energy levels within the cluster, while N_D and N_T are the external shallow donor density and cluster recombination center density, respectively. Gregory[21] showed that the space-charge in the neighborhood of the cluster creates a disturbance in the electrostatic potential which places the recombination center inside the cluster at the top of a potential hill with respect to the majority carriers, and at the bottom of a potential well with respect to the minority carriers. His calculations[20] for the build-up of charge within the cluster following a large pulse of injected minority carriers predicted that the excess conductivity produced by this pulse should decay at an extremely slow nonexponential rate. Gregory's calculations were performed for 10 ohm-cm n-type silicon with a cluster density of 5.9×10^{12} cm^{-3}. The cluster parameters employed were $R_1 = 250$ Å, $N_T = 5.19 \times 10^{17}$ cm^{-3} (34 defects/cluster), $E_{TD} = E_v + 0.35$ eV and $E_{TA} = E_c - 0.5$ eV. Minority carrier recombination studies also conducted by Gregory[20] showed that the height of the potential barrier produced by the defect cluster was the key factor in determining its influence on minority carrier recombination. The parameters which Gregory considered most important in determining this barrier were:

1. The defect energy levels in the cluster,
2. The number of defects in the cluster,
3. The cluster size,
4. The majority dopant density in the surrounding undamaged material.

The parameters which best fit the data were obtained for a cluster size of $R_1 = 250$ Å containing a fairly small number of defects (30 to 40). The other significant parameters were $E_{TD} = E_v + 0.35$ eV, $E_{TA} = E_c - 0.50$ eV, $\sigma_{ND} = \sigma_{PA} = 4 \times 10^{-15}$ (300/T) cm^2 and $\sigma_{PD} = \sigma_{NA} = 4 \times 10^{-16}$ (300/T) cm^2, where σ_{ND}, σ_{PD}, σ_{NA} and σ_{PA} are the electron and hole capture cross sections for the donor and acceptor levels, respectively. Due to the deep donor level near $E_v + 0.35$ eV and a deep acceptor level near $E_c - 0.50$ eV, Gregory proposed that the divacancy may be the active recombination center within the defect clusters. The divacancy is known to have a deep donor and acceptor at these respective levels[22,23] as well as a double acceptor near $E_c - 0.40$ eV. Wilson,[24] in earlier work, had also found majority carrier traps in p^+n silicon diodes at the $E_v + 0.36$ eV level with a cross section of roughly 10^{-15} cm^2.

A trap level has also been suggested at $E_v + 0.31$ eV as a result of experiments conducted on high resistivity n-type, tin-doped gallium arsenide.[25]

The two major effects of neutron displacement damage to semiconductor material can be given by two simple equations.[4] One equation relates the change in the recombination rate to a function of the radiation exposure:

$$R = 1/\tau = 1/\tau_o + K\emptyset \ , \qquad (2.1)$$

where R and $1/\tau$ are the recombination rate per carrier and minority carrier lifetime, respectively after irradiation, $1/\tau_o$ is the minority carrier lifetime before radiation, $\emptyset$ is the radiation exposure in units of neutrons per square centimeter (n/cm^2), and K is the radiation

damage constant or coefficient (cm^2/n-sec). The second equation,

$$N = N_o - (dN/d\phi)\,\phi \ , \qquad (2.2)$$

gives the change in impurity concentration as a function of exposure. The coefficient $(dN/d\phi)$ is called the carrier removal rate in units of carries/n-cm, and N_o is the impurity concentration (cm^{-3}) prior to exposure.

A. TRAPATT Devices

The most practical method of starting TRAPATT oscillations is to make use of the small signal negative resistance inherent in the IMPATT mode of the diode.[10] Due to the IMPATT frequency being considerably higher than the TRAPATT frequency, a pulse with sufficient rise time will be generated to launch an avalanche zone into the depletion region, provided the RF voltage builds up to sufficient amplitude.[9,10] It is therefore apparent that the effects of neutron exposure on the IMPATT mode of operation should also be considered in analyzing effects on TRAPATT devices.

Measurements and studies have been made to determine the effects of neutron radiation on IMPATT and TRAPATT performance.[26-35] Experiments were carried out by Chaffin and EerNisse[29,32,35] on TRAPATT devices. They performed calculations[32] which described the avalanching p^+nn^+ junction in the presence of multiple-level carrier traps produced by neutron irradiation and compared these results with experimentally observed data from TRAPATT and IMPATT studies.[27,29] The significant results of this study was the method in which the electric field and space-charge density within the device were perturbed with increasing trap concentration. With an assumed doping profile, shown

in Fig. 2.2, the perturbation in the electric field can be seen in Fig. 2.3. The avalanche region begins to localize on the p^+n side of the space-charge region. Avalanching occurs at greater fields when the trap concentration exceeds the donor concentration.[32] The density of trapped charge in the charged states of the multiple-level traps are shown in Figs. 2.4 and 2.5 for increasing trap densities. Even though the space-charge region for TRAPATT operation is different than that shown here for IMPATT operation, the electric field should tend to be perturbed in the same direction.[32] The measured changes in the DC operating voltages for two abrupt junction TRAPATT samples (12 micron deep p^+ diffusion into a silicon nn^+ epitaxial layer) are plotted with the calculated changes of the IMPATT mode in Fig. 2.6. The authors indicated that the increase in DC operating voltage necessary to maintain a given current density occurs when the space-charge region is extended at the edges due to large trap concentrations. Measurements and calculations made[35] on two other TRAPATT devices (25 micron deep diffusions from both sides of the silicon wafer) reflected that these were less resistant to breakdown voltage increases with neutron fluence than were the more abrupt samples. It was further indicated[32] that when the trapping concentrations become large enough, the excess carrier lifetime (0.7 ns for 6×10^{15} n/cm^2 and 1000 A/cm^2) in the avalanche region becomes comparable with the transit time (approximately 0.1 ns) and losses are introduced. This effect can be seen in Fig. 2.7 where the time (relative to the pre-irradiation values) for the IMPATT mode to build up to a level sufficient to trigger the first TRAPATT oscillation is plotted versus

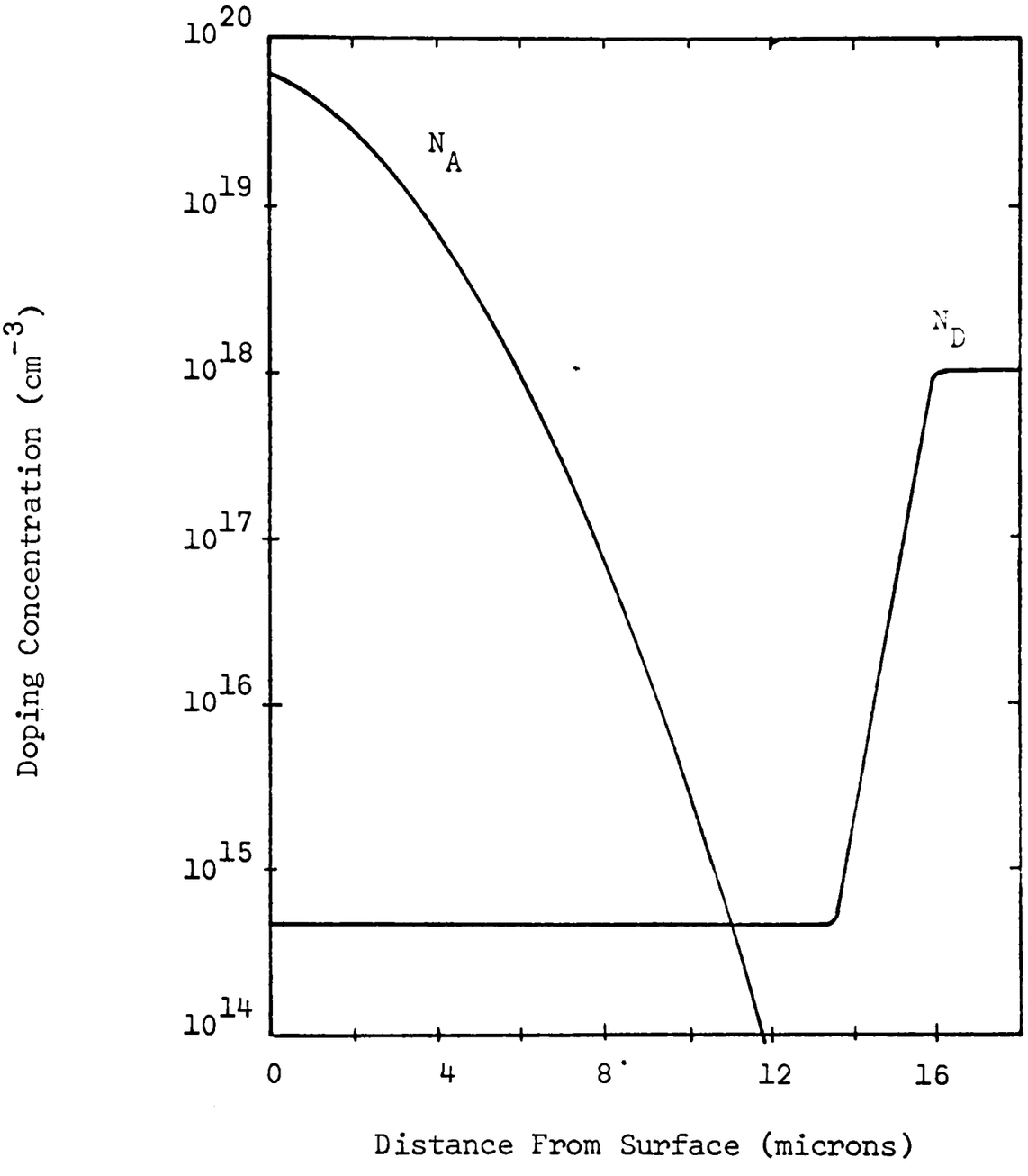

Figure 2.2. Doping profile used in calculations pertaining to avalanching p^+nn^+ junction. (After EerNisse and Chaffin.[32])

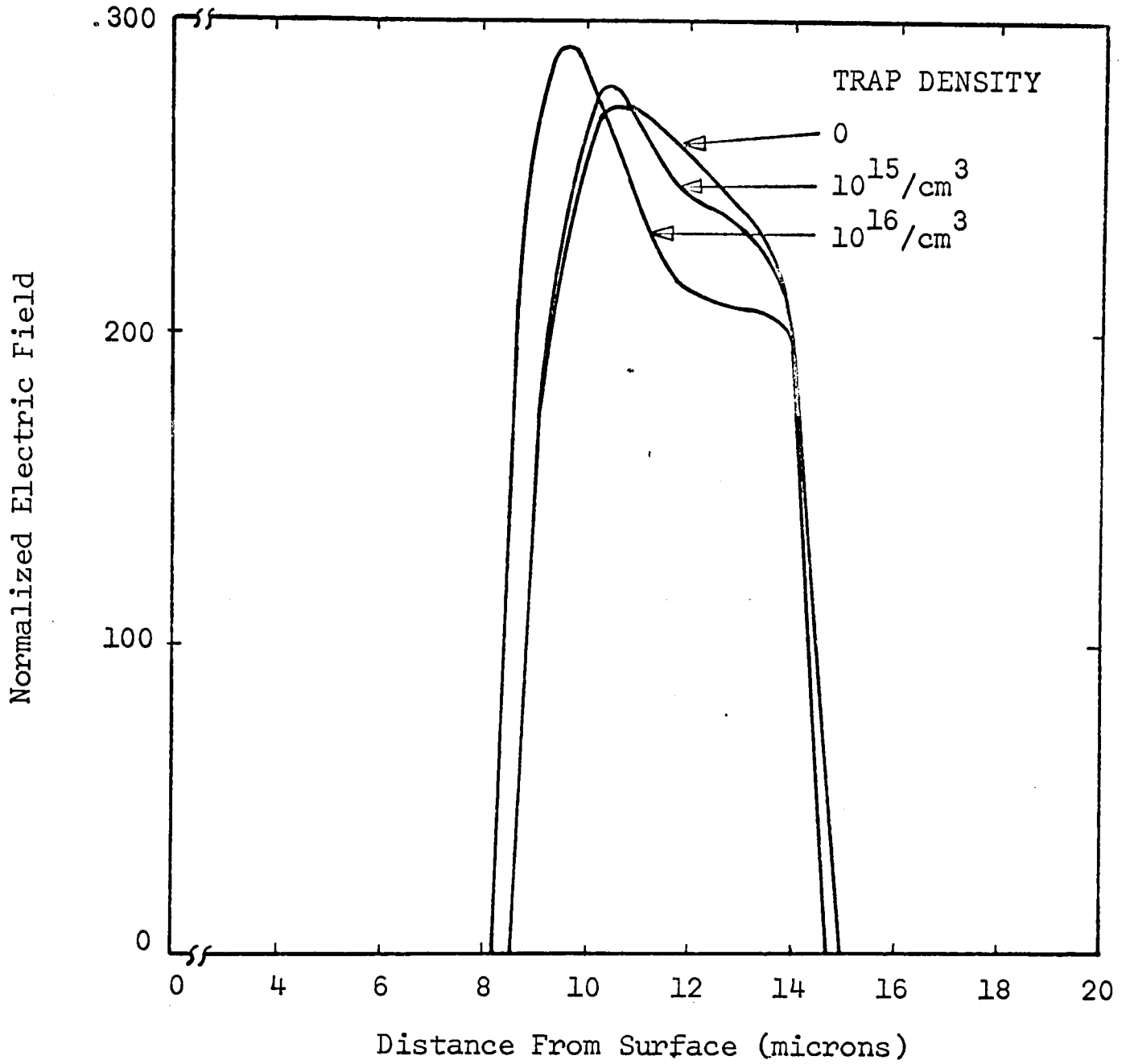

Figure 2.3. Perturbation in electric field due to carrier trapping calculated for device biased into avalanche breakdown at 100 A/cm^2. (After EerNisse and Chaffin.[32])

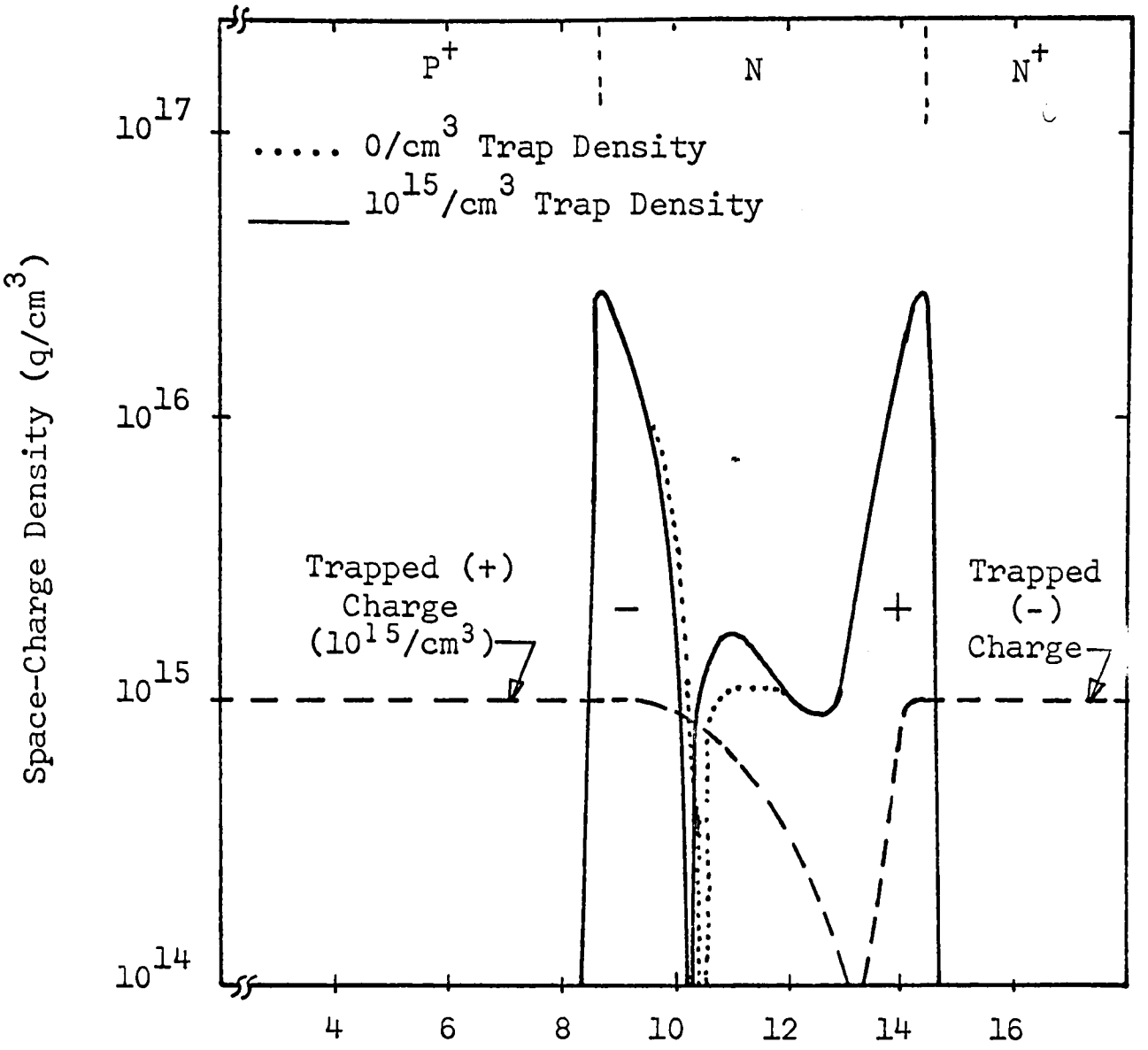

Figure 2.4. Space-charge density versus distance from junction calculated for device biased into avalanche breakdown at 1000 A/cm^2 for trap density of 10^{15}/cm^3. (After EerNisse and Chaffin.[32])

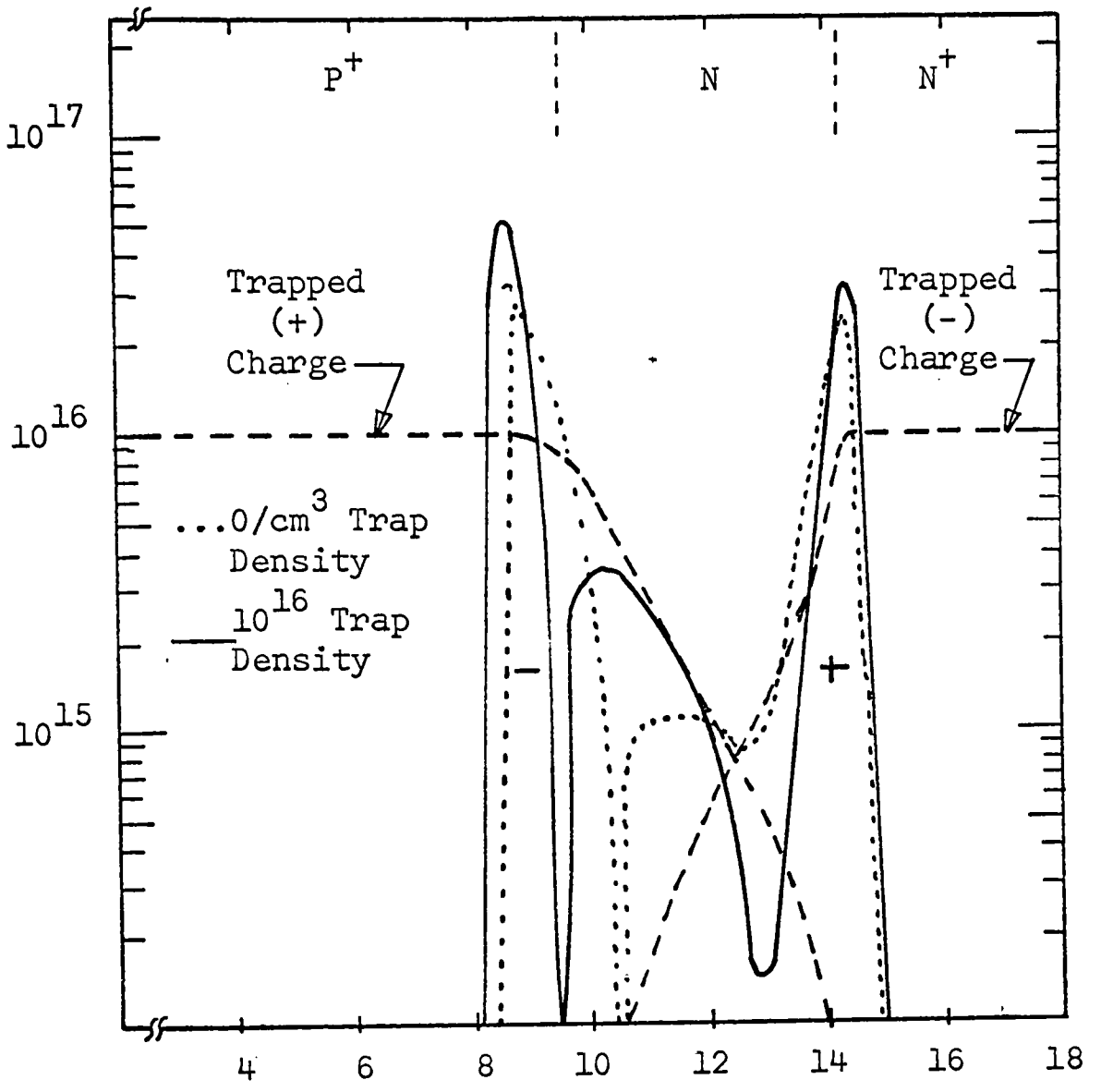

Figure 2.5. Space-charge density versus distance from junction calculated for device biased into avalanche breakdown at 1000 A/cm^2 for trap density of 10^{16}/cm^3. (After EerNisse and Chaffin.[32])

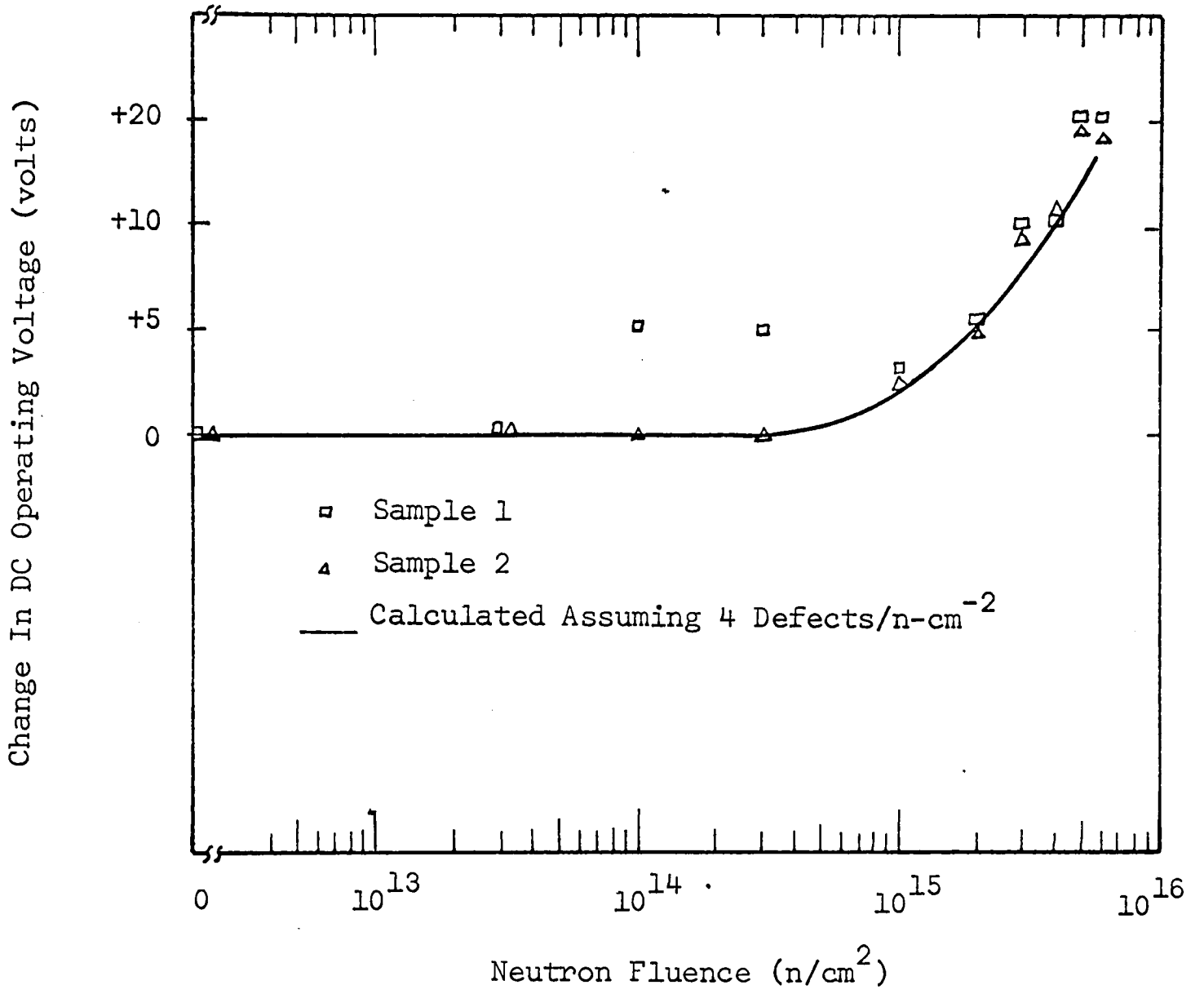

Figure 2.6. Measured changes in DC operating voltage for TRAPATT and calculated changes for IMPATT device at 1000 A/cm^3 assuming 4 defects per n/cm^2. (After EerNisse and Chaffin.[32])

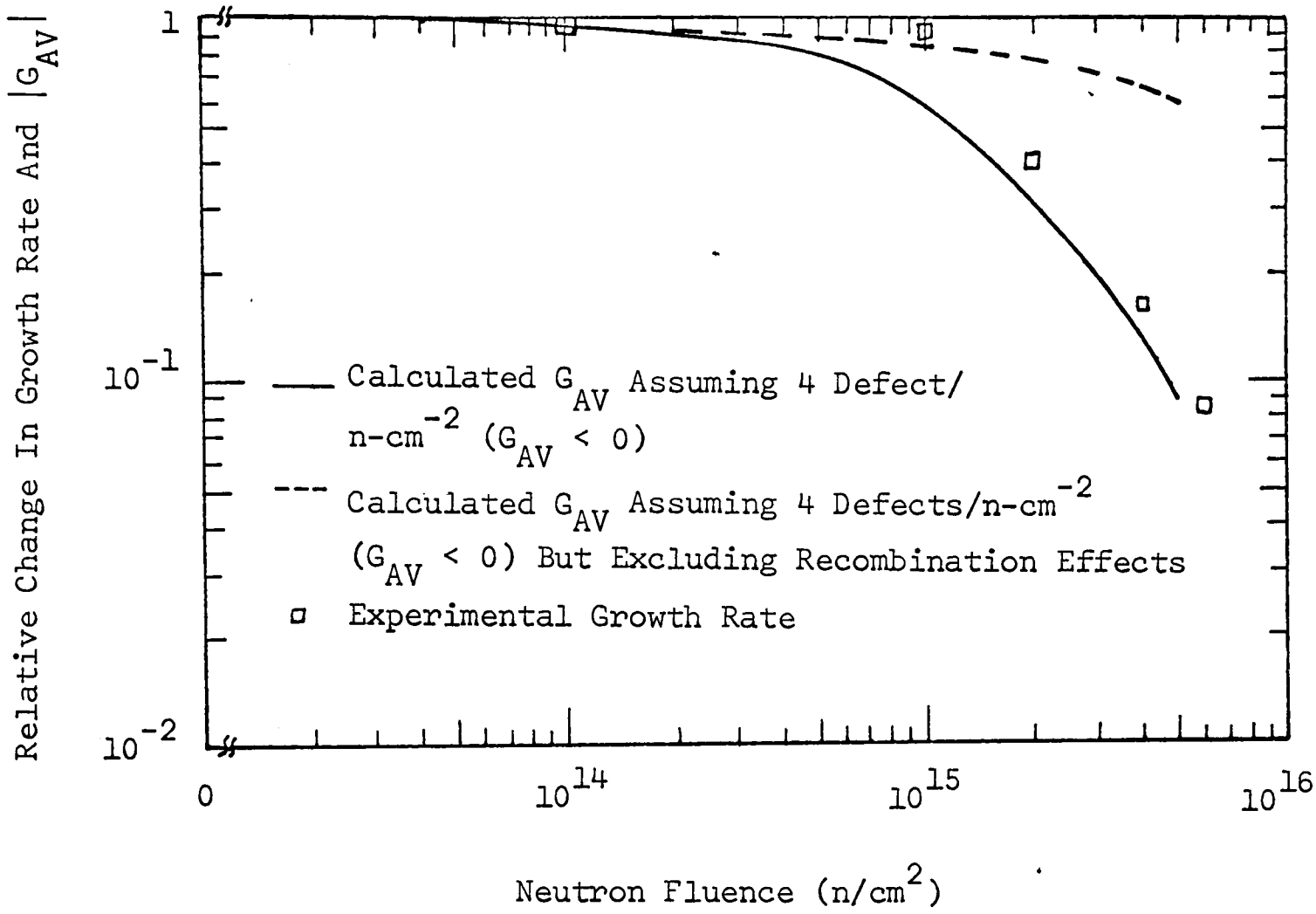

Figure 2.7. Calculated and measured time for IMPATT signal to build up to a sufficient level to trigger the TRAPATT oscillation. (After EerNisse and Chaffin.[32])

neutrons/cm^2 along with the calculated negative conductance (normalized to the pre-irradiation level) introduced into the cavity in the 2 to 7 GHz frequency range by avalanche and transit time effects G_{AV}.[32] The small-signal IMPATT growth rate is degradated because some of the carriers injected by the avalanche process recombine as they transit the space-charge region. The solid line demonstrates the importance of including recombination effects in calculations with the continuity equations. These carrier recombination effects combined with the localization of the avalanche region on the p^+n side of the space-charge region can be considered as the cause of failure of both IMPATT and TRAPATT diodes.

When the time required to build up the IMPATT mode to a sufficient level to trigger the TRAPATT oscillations is increased, then the amount of time that the bias pulse is applied to the device is decreased.[35] This results in a reduced average power output from the device which can be seen in Fig. 2.8 for both the abrupt and deep diffused junction devices. The results reflect no degradation in power up to 10^{15} neutrons/cm^2 and a drastic decrease near 6×10^{15} neutrons/cm^2 for the abrupt junction devices. The deep diffused devices showed degradation at fluences greater than 10^{14} neutrons/cm^2. The abrupt junction devices indicated more resistance to neutron damage; however, the degradation in average power was due to the difference in depletion widths of the two devices.[35] The unirradiated abrupt junction devices had a depletion width of 6 microns (for 1 GHz operation); whereas, the diffused junction had a 10 micron (for 600 MHz operation) depletion width.

Experimental data on the abrupt junction TRAPATT device reflected

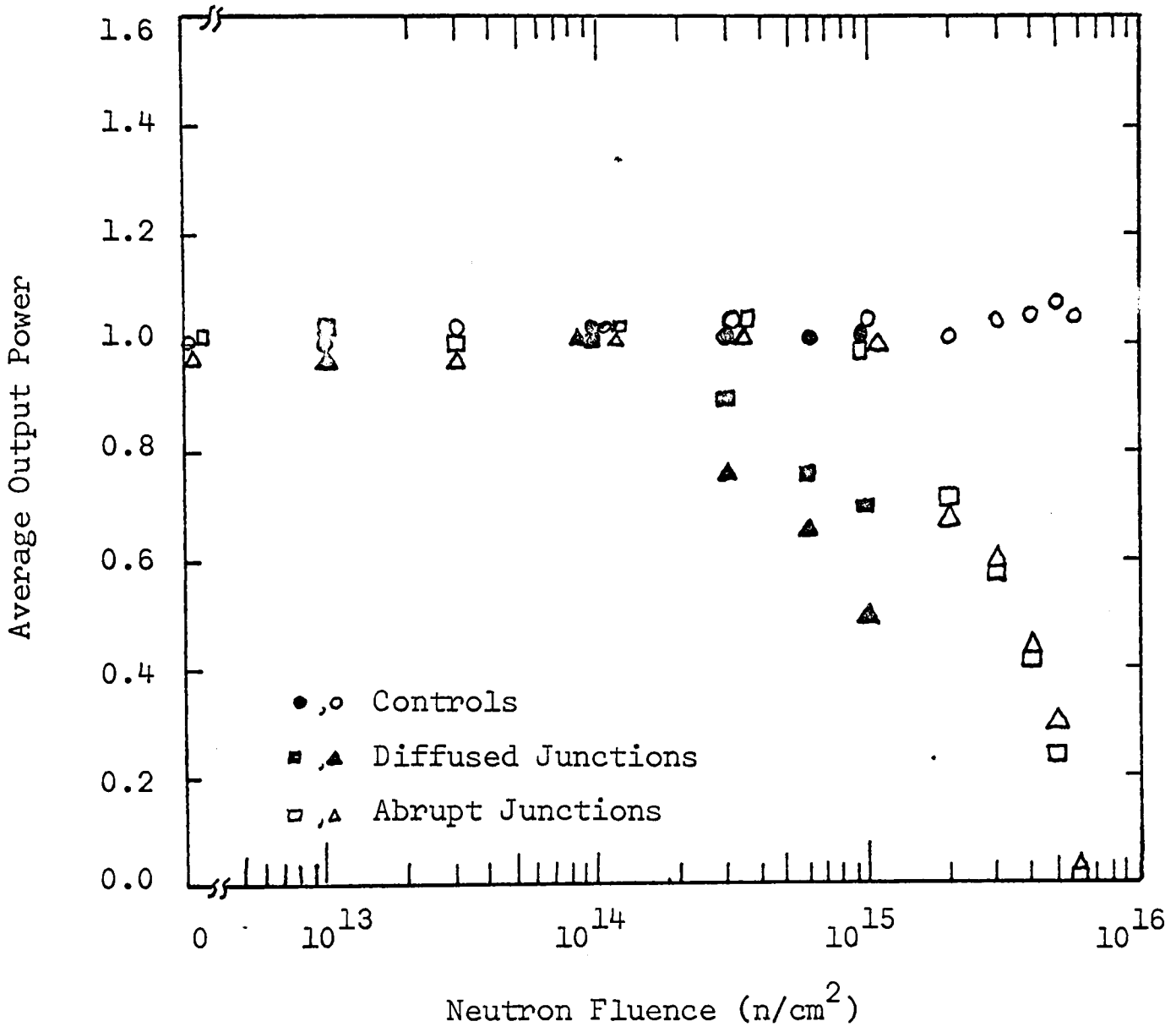

Figure 2.8. Average output power normalized to pre-irradiation values versus neutron fluence for abrupt and diffused junction devices. (After EerNisse and Chaffin.[35])

only a slight change in frequency at fluences greater than 10^{14} n/cm^2.[32,35] The change was approximately 1 percent at 6×10^{16} n/cm^2 and was attributed to localization of the avalanche zone near the p^+n side of the device by carrier trapping in the n-region.

EerNisse[31] has further shown the existence of negative temperature coefficients of the breakdown voltage in irradiated devices with other than abrupt junctions. The negative temperature coefficient gives rise to a negative resistance in the avalanche region.[26] The temperature coefficient is generally given by $V^{-1}\partial V/\partial T$ for a given current density at a given temperature T, where V is the voltage across the device. The carrier extraction at the edges of the space-charge region is reduced with an increase in temperature because of increased thermal release of trapped charge resulting in a negative contribution to the diode temperature coefficient.[31,35] Experimental data supported his calculations that for higher trap density, a higher current density was necessary to cause the positive coefficient of avalanche generation to dominate. As can be seen in Fig. 2.9, the more abrupt junction device will reduce the negative temperature coefficient resulting in a more radiation resistant device.[35] A device with a negative temperature coefficient implies current filament formation resulting in possible destruction as the neutron fluence is increased.

Wilson, et al,[26] measured the minority carrier lifetime for an abrupt epitaxial p^+nn^+, X-band, silicon avalanche diode consisting of a 7 micron epitaxial n-layer with 10^{16} cm^{-3} donors deposited on a heavily doped n-type substrate. The results obtained can be fitted

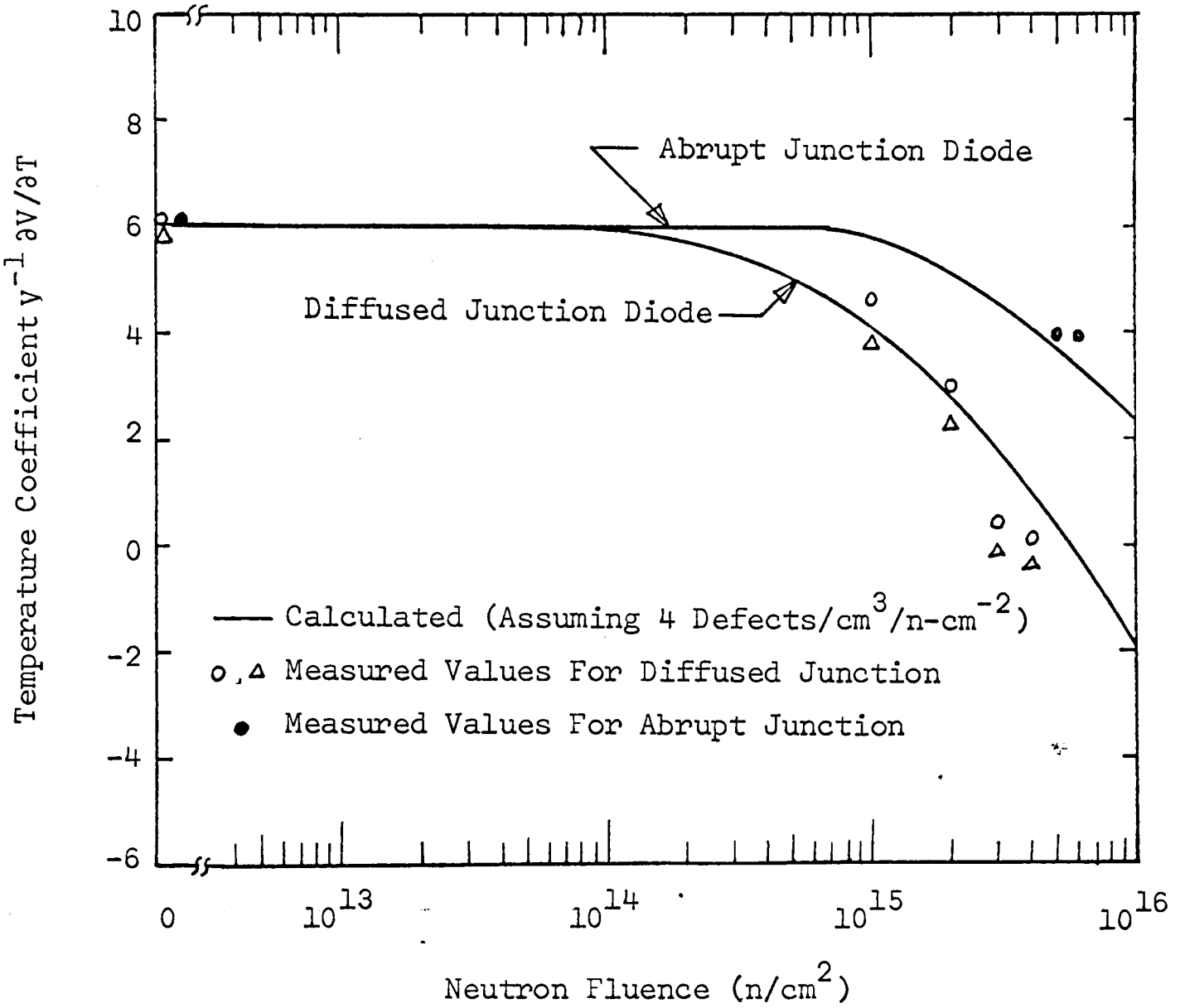

Figure 2.9. Calculated and measured temperature coefficient at 30 A/cm^2 versus neutron fluence for abrupt and diffused junction devices. (After EerNisse and Chaffin.[35])

to Eq. (2.1) with a radiation damage constant of $K = 0.7 \times 10^{-6}$ cm^2/(n-sec).

DC measurements of the avalanche breakdown region as a function of neutron fluence were made on an IMPATT device,[26] and it was found that the breakdown characteristics were affected very little for fluences of up to 10^{15} n/cm^2. Between 10^{15} n/cm^2 and 10^{16} n/cm^2, however, the concentration of active defects approached the impurity concentration causing a significant increase in breakdown voltage which indicated that approximately 0.5 donors/n-cm were removed in the space-charge region at 10^{16} n/cm^2.[26]

Junction capacitance measurements made by Wilson, et al,[26] indicated little change up to 10^{15} n/cm^2. At greater fluences, a large decrease in capacitance was noted and attributed to the formation of a narrow intrinsic region at the p^+n junction.[26] Wilson, et al, further indicated that a decrease in majority carrier dopant at a rate of 0.5 carriers/n-cm was also noted by these measurements.

The carrier removal rate noted by Wilson, et al,[26] is less than that assumed by Larin in his calculations. Larin indicated that measured values for n-type silicon were between 1.0 and 4.0 carriers/n-cm and used the value 1.3 for impurity concentrations near 10^{15} cm^{-3}. The lower value of 0.5 found by Wilson, et al, can probably be attributed to the high purity, epitaxial grown silicon material used in the IMPATT diodes.

Buehler[36] proposed a model describing the space-charge region of silicon p^+n junction in the presence of deep traps. The model was applied to high frequency (1 MHz) capacitance-voltage measurements of two neutron irradiated silicon p^+n junction. Buehler indicated, as

have other investigators, that the divacancy is a defect to be expected in such devices. He also found that the defect introduction rate at room temperature for one of the junctions fabricated in epitaxial material (N_D = 5 x 10^{14} cm^{-3}) was 0.64 cm^{-1} and was less than that found for bulk material (0.95 cm^{-1}). Buehler further observed that the space-charge width is increased by deep traps with the amount of increase dependent upon the trap and background concentration.

Lithium has been used in silicon solar cells to achieve radiation resistance. Lithium acts as an interstitial donor and displays considerable mobility; while, conventional dopants like phosphorus or arsenic occupy substitutional lattice positions and are relatively immobile.[37] Lithium doped silicon material, however, has exhibited significantly higher carrier removal rates (7 to 75 carriers/n-cm) than phosphorus doped samples (6 to 12 carriers/n-cm) at carrier concentrations from 10^{13} to 10^{16} cm^{-3} when exposed to 5 MeV neutrons.[37] The lithium doped samples reflected a strong dependence of the carrier removal rate on the dopant concentration, while phosphorus samples were relatively independent of dopant level. The high carrier removal rates in lithium samples were suggested by Kimerling and Drevinsky[37] as resulting from a loss of lithium donors as electrically active entities as compared to the compensation of conduction electrons responsible in conventionally doped samples. The removal rates found for phosphorus were higher than had been previously reported and were attributed by Kimerling and Drevinsky to the higher neutron energy (5 MeV) used in their investigations.

B. LSA Devices

Gallium arsenide has emerged within the past decade as an operational source for solid-state power devices. The compound is not as well known as silicon and germanium. However, its potential application in microwave generators has developed considerable interest in determining its use in a nuclear environment.

The effects of neutron irradiation have been studied[33,34,38-41] and indicate that carrier removal is the primary cause of failure in devices composed of gallium arsenide. Gunn effect devices seem to fail due to a too small doping-length product, while LSA devices fail due to an increase in low field DC resistance, R_o, with increasing neutron fluence. The low field resistance can be obtained from

$$R_o = L/(eNA\mu), \tag{2.3}$$

where L is the diode length, A is the diode area, N is the carrier concentration, e is the electron charge, and μ is the electron mobility. Berg and Dropkin[38] found, through tests conducted on epitaxially grown gallium arsenide samples, that an induced change of mobility resulted, whose magnitude varied linearly with donor impurity density and the pre-irradiated value of mobility and varied inversely with fluence. Their experiments resulted in the approximation[38]

$$1/\mu_f \tilde{=} 1/\mu_o + (2.7\ \phi)/N_D\mu_o), \tag{2.4}$$

where N_D is the donor impurity density, and μ_f and μ_o are the post-irradiation and pre-irradiation values of mobility, respectively. The decrease in mobility had been assumed negligible by some investigators in calculating the carrier concentration[39] and low field resistance[33] at fluences as large as 10^{14} n/cm^2. Marcus and Bruemmer[39] experimentally

determined the carrier removal rate in gallium arsenide, assuming constant mobility, using

$$N \tilde{=} N_o R_o / R(\emptyset) \ , \tag{2.5}$$

where N_o and R_o are the pre-irradiated values of carrier concentration and low field resistance, respectively, and $R(\emptyset)$ is the resistance at fluence, $\emptyset$. The carrier removal rate was calculated and determined to fit the equation

$$dN/d\emptyset \tilde{=} 9.08 \times 10^{-6} N_o^{0.4} \ , \tag{2.6}$$

as shown in Fig. 2.10.[39]

Chaffin[33] measured the change in low field resistance of a gallium arsenide Gunn diode, having a doping concentration in the active region of 8×10^{14} cm^{-3}, after neutron exposure from the Sandia Pulsed Reactor-II. The resistance changes from a pre-irradiated value of 5 ohms to a value of 80 ohms at 10^{14} n/cm^2, as shown in Fig. 2.11.

Wilson and Gregory later studied the effects of neutron damage in oversized epitaxial gallium arsenide diodes operated in the LSA mode.[40,41] Two lots of diodes were tested having the following characteristics:

	Lot 1	Lot 2
Carrier concentration, N, (cm^{-3})	1.4×10^{15}	2.7×10^{15}
Mobility, μ, (cm^2-volt^{-1}-sec^{-1})	7900	7900
Diode length, L, (cm)	0.008	0.011
Low field resistance, R_o, (ohms)	1.5-2.0	1.2-1.8

The results of the test, using the Sandia Pulsed Reactor-II, can be seen in Table 1. The low field resistance of Lot 1 only increased 80 percent and was a smaller increase than that reported by Caffin.[33]

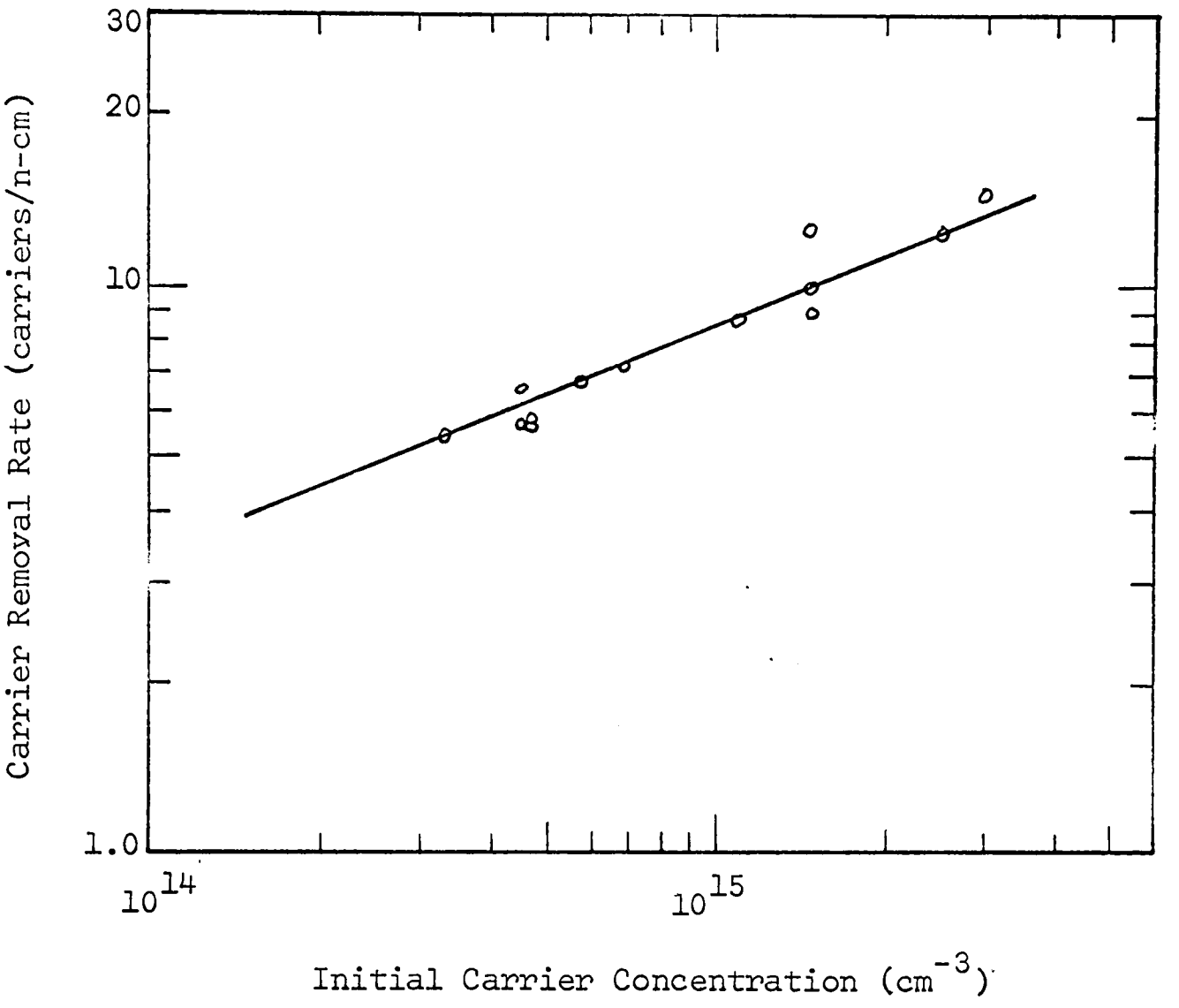

Figure 2.10. Carrier removal rate versus initial carrier concentration. (After Marcus and Bruemmer.[39])

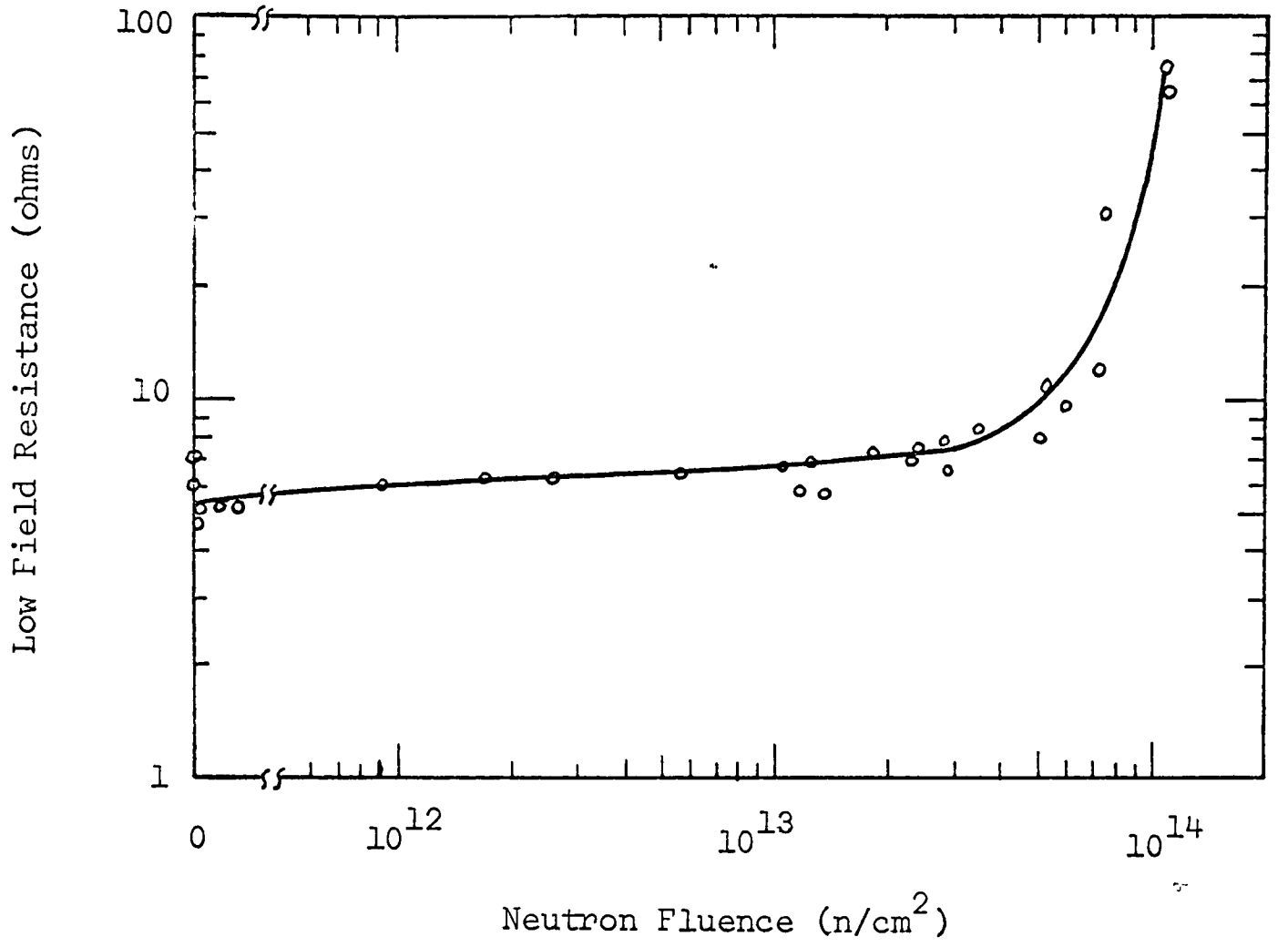

Figure 2.11. Low field resistance versus neutron fluence for Gunn diode. (After Chaffin.[33])

TABLE 2.1

Results of measurements concerning low field resistance and mobility and calculated values of carrier removal made by Wilson and Gregory[41] with increased neutron fluence.

Wafer	$\phi \times 10^{13}$	$\Delta R_o/R_o$	$\Delta\mu/\mu$	$dN/d\phi$
Lot 1	1.0	0.05	--	--
	3.0	0.15	0.031	4.7
	7.3	0.38	0.066	4.5
	11.3	0.80	0.139	4.7
Lot 2	10.0	0.38	0.09 est	7.8 est

However, this difference is probably due to the different carrier concentrations of each device. The changes in both low field resistance and mobility were used in calculating the carrier removal rate and is a smaller value (4.6 carriers/n-cm) than that which can be estimated by Eq. (2.6) (approximately 10 carriers/n-cm). Caffin's data, however, agrees with the approximation developed by Marcus and Bruemmer.[39]

The frequency of the LSA oscillators increased for a fixed bias level due to a dependence on the diode low field resistance determined from[41]

$$f = \left[2\pi\sqrt{LC} + \frac{L}{R_o} \left(\frac{\alpha - 1}{M\alpha - 1} \right) \right]^{-1} , \qquad (2.7)$$

where L and C are the equivalent microwave inductance and capacitance, respectively, M is the operating-to-threshold voltage ratio V_b/V_t and α is the current peak-to-valley ratio I_p/I_v. The values for L, C, and α remained unchanged with neutron fluence.[41] The change in frequency, for fixed bias, determined by Wilson for the diodes from Lot 1 is shown in Fig. 2.12.

The diode breakdown voltage (maximum bias voltage) also was found by Wilson to decrease rapidly with fluence.[41] The reduced breakdown voltage was attributed to carrier removal resulting in a lower N/f value causing domain formation[40] before the RF voltage had time to swing below threshold. The maximum allowable bias voltage M_{max} was expressed as

$$M_{max} \tilde{=} (\alpha - 1)R_L/(\alpha\ 2AR_o) , \qquad (2.8)$$

where R_L is the load resistance seen by the diode and A is a constant

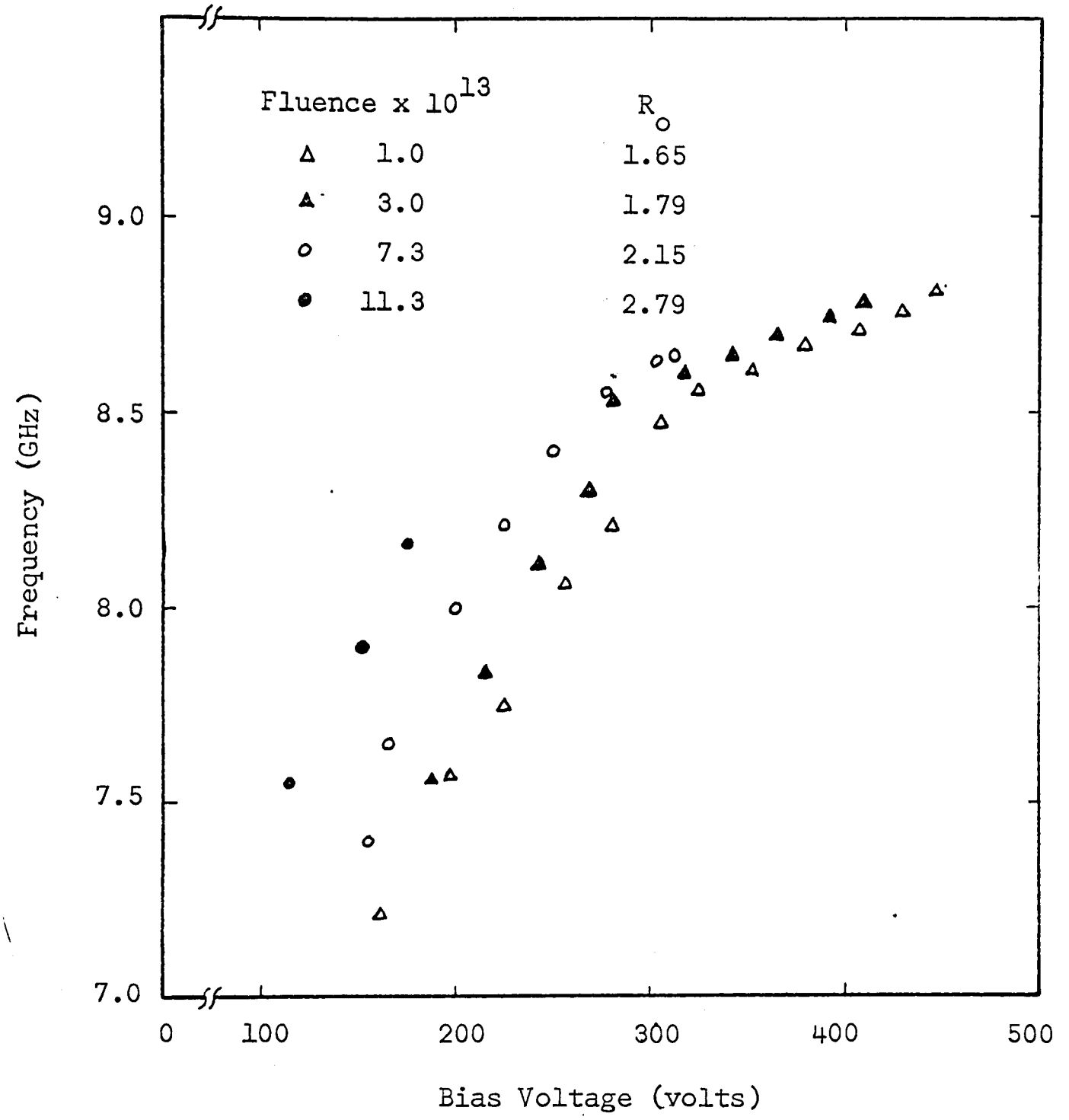

Figure 2.12. Change in frequency as a function of bias voltage. (After Wilson.[41])

related to the RF current waveform near breakdown.[40,41]

Wilson and Gregory also found that the threshold voltage and oscillation power output remained essentially unchanged with neutron fluence for a fixed bias voltage.

C. Device Configuration

TRAPATT and LSA oscillators have been designed and tested in both waveguide cavity, stripline and microstrip circuits. Waveguide cavity mounts will not be affected by neutron exposure; however, stripline and microstrip dielectric material, which is a critical factor in the proper performance of all strip circuits, has been studied[42] to determine whether or not this material is affected. Any effect of neutron irradiation on the dielectric constant of the material could be a critical factor in the proper performance of any strip circuit since this material property controls or affects all circuit parameters. The engineering and effort applied to the development of a reliable, low loss, and dimensionally stable stripline base has also resulted, in some cases, in a material resistant to neutron radiation.

Alumina, sapphire and fiberglass reinforced teflon are three of the most common substrate materials used in stripline and microstrip circuits and were investigated[42] by Wilson and Chaffin for permanent radiation damage. Microstrip and stripline bandpass resonator circuits were used in the test to provide information regarding the stability of the complex permittivity and mechanical stability of the substrates. The investigation showed no change in microwave properties of the three types of substrates after exposure to 2×10^{15} n/cm^2.[42]

CHAPTER III

GAMMA RADIATION EFFECTS

Gamma rays lose their energy in matter by ionizing interactions. The primary processes that need to be considered here are those that cause electrons to be removed from atoms and not those resulting in the displacement of whole atoms. The electron-ion pairs, however, are not formed entirely by the incident gamma rays. Many secondary electrons produced from gamma ray interactions with semiconductor material and from interactions with other material penetrated prior to reaching the electrical components of a system also have sufficient energy to produce further ionization.

Gamma rays interact with matter through the photoelectric process, pair production process, and the Compton effect.[5] Gamma rays with energies of 0.1 MeV are mostly in the photoelectric regime.[19] In this process, a ray is absorbed by a target atom, and most of its energy converted into kinetic energy of a secondary electron which produces ionization.[5] Gamma rays with energies of 0.7 to 2 MeV, emitted during a fission process, interact mostly through the Compton process.[19] In this process, the gamma ray is scattered by an electron, and some of the energy of the gamma ray is lost to the electron.[5] The less energetic, scattered gamma ray may further interact with matter through the Compton or photoelectic processes. The more energetic electrons involved in the scattering event can produce ionization. Gamma rays with energies greater than approximately 2 MeV interact through the pair production process where the gamma ray is absorbed

by an atom and its energy is converted into an electron-hole pair. The Compton process, however, is the primary energy-loss mechanism in a fission weapon environment, particularly in materials having low atomic numbers.[5]

The rate of energy deposition within a material, from an incident gamma ray, increases from the surface inward and reaches a maximum at a distance depending upon the range of the average-energy secondary electrons and at the point where the rate of secondary electron generation equals the rate the electrons are removed by ionization energy loss.[5] It was pointed out by van Lint[5] that the gamma rays will have already interacted with other materials before reaching circuit components, which will have created a gamma-electron equilibrium that will not be changed very much on entering electrical components.

The result of the ionization processes discussed above depends on the secondary interactions of the electrons and holes which include diffusion, drift, trapping and recombination. The effects most concerned with in this thesis are those resulting from an increase in carrier concentration. The increase in carrier concentration can be determined by adding a carrier generation term to the continuity equation. The rate of variation of minority carriers or holes, p, in an n-type sample can be expressed as

$$\frac{\partial \Delta p}{\partial t} = G_p - \frac{(p_n - p_{no})}{\tau_p} - \frac{1}{q} \operatorname{div} \bar{J}_p \quad , \tag{3.1}$$

where G_p is the hole generation rate (carriers-cm^{-3}-sec^{-1}) due to external influences such as impact ionization and gamma radiation. The hole recombination rate is expressed as $(p_n - p_{no})/\tau_p$ since the injected carrier density is much less than the equilibrium majority

carrier density. The quantity p_n is the minority carrier density, p_{no} the thermal equilibrium minority carrier density, and τ_p the minority carrier lifetime. $\bar{J}_p$ is the hole current density vector quantity. There is a similar expression for the variation of majority carriers. If the electrons and holes are generated and recombined in pairs with no trapping or other effects then $\tau_p = \tau_n$. When gamma radiation is the only external influence on the carrier generation rate, then

$$G_p = g_o \dot{\gamma}, \tag{3.2}$$

where g_o is the carrier generation rate conversion factor (carriers-cm^{-3}-rad^{-1}) and $\dot{\gamma}$ is the radiation energy deposition rate (rads/sec). The conversion factor, g_o, is determined from the material density and the amount of radiation energy required to produce one hole-electron pair. Since 3.6 eV[4] is required to generate a single electron-hole pair in silicon which has a density of 2.33 g/cm^3, the conversion factor can be calculated[4] as

$$g_o = \frac{\left(\frac{100 \text{ ergs}}{\text{g-rad}}\right)\left(\frac{2.33 \text{ g}}{\text{cm}^3}\right)}{\left(\frac{10^7 \text{ ergs}}{\text{J}}\right)\left(\frac{1.6 \times 10^{-19} \text{J}}{\text{eV}}\right)\left(\frac{3.6 \text{ eV}}{\text{carriers}}\right)}$$

$$= 4 \times 10^{13} \text{ carriers/cm}^3\text{-rad}. \tag{3.3}$$

Gallium arsenide having a density of 5.32 g/cm^3 requires[43] 4.6 eV to generate a single electron-hole pair which results in a conversion factor of 7.25×10^{13} carriers/cm^3-rad. The 4.6 eV value, however, does not correlate well with intrinsic ionization within the material.

The use of the simple relationship between carrier concentration

and ionizing radiation to permit a direct conversion from radiation to parameters of interest in semiconductor devices depends upon the width of the ionization pulse in relation to pertinent relaxation times.

An ionization pulse which is wide compared to all of the pertinent relaxation times results in steady-state effects which may include excess photocurrents in a pn junction or excess conductivity in semiconductors.[5] The magnitude of the effect is a function of the instantaneous excess carrier density, ΔN, which is a function of the generation rate, G_p, as

$$\Delta N = G_p \tau \ . \tag{3.4}$$

The increase in carrier density results in an increase in conductivity which can be determined from

$$\Delta\sigma = eg_o\dot{\gamma}\tau(\mu_n + \mu_p) \ , \tag{3.5}$$

since electrons and holes have comparable mobilities in semiconductors.

An ionization pulse which is short compared to pertinent relaxation times results in delayed effects in which the initial response is primarily a function of total dose, γ, and its persistence is determined by the relaxation time.[5] In this case, the increase in conductivity of a semiconductor rises while the pulse is applied, and at the end of the pulse decays exponentially depending upon the value of the minority carrier lifetime. The maximum value of the conductivity change can be determined[5] from

$$\Delta\sigma_m = eg_o\gamma(\mu_n + \mu_p) \ . \tag{3.6}$$

The effects of gamma ray exposure, previously mentioned, are transient in nature due to electrons being excited or ionized. These

effects usually produce significant changes only in the electrical and optical properties of materials, and except for very large doses of radiation, the perturbations which would affect device operation are short lived. A large amount of high-energy gamma rays can produce displaced atoms by first generating secondary electrons which then produce the atomic displacements. The atomic displacement effect is a permanent damage, but is not as severe as that produced by the heavier neutron particles. As an example, Brehm and Pearson[44] proposed that point defects were introduced into gallium arsenide by gamma ray exposure. These point defects had energy levels within the forbidden gap which trapped free electrons at the rate of approximately one electron per defect. Chaffin[33] later determined the carrier removal rate for gamma rays to be approximately 0.8×10^{7} cm^{-3}-rad^{-1} from the results obtained by Brehm and Pearson. Using neutron and gamma ray defect introduction rates of 3 and 0.006 cm^{-1} respectively for gallium arsenide, Brehm and Pearson determined that the ratio of photons required to produce a given carrier removal to neutrons required to produce the same carrier removal was 500.

A. TRAPATT Devices

Experimental results published, thus far, pertaining to gamma radiation effects of avalanche devices have been concerned with IMPATT diodes. There is disagreement between workers. Although data has not been published concerning the TRAPATT mode, the IMPATT results are useful since it was pointed out in Chapter II that the IMPATT mode is the most practical method of starting TRAPATT oscillations. One would expect, however, a higher tolerance to gamma radiation due to the

on-off switching mechanism of the TRAPATT oscillator.[45]

Anderson[30] tested a 3 milliwatt, X-band diode with 15 msec pulses of both neutron and gamma radiation. The diode ceased to oscillate during and immediately after each pulse with the lowest radiation exposure being 1.95×10^{15} n/cm^2-sec and 2.73×10^6 rads/sec. He reported that partial recovery of oscillation occured after a 15 minute period, and that full oscillator recovery occured after the bias voltage was reduced to zero and then increased to the proper level. Anderson believed that the electron-hole pair formation produced a current pulse of sufficient magnitude to disrupt the avalanche process. He contributed the slow recovery time to diode being self-radioactive immediately after irradiation.

Anderson[34] later tested both passivated (by thermal oxidation) and unpassivated X-band IMPATT diodes. His results indicated that the passivated diodes were less tolerant to gamma radiation than the unpassivated ones. Anderson also measured the change in reverse bias current at fixed reverse bias voltages with changes in temperature and radiation exposure. These results are shown in Fig. 3.1. Curve 3 shows the increase in current during radiation exposure and is greater than the temperature effect alone. Anderson indicated that curve 4 was obtained shortly after the reactor test with the sample still in a small gamma flux and that carrier generation was still present due to self-radioactivity of the diode and cavity.

Chaffin[33] tested 100 milliwatt, 11 GHz, CW operated IMPATT oscillators at dose rates of 7.4×10^6 rads/sec, 7.0×10^7 rads/sec, and 5.4×10^8 rads/sec. The diodes were unpassivated, p^+nn^+, silicon

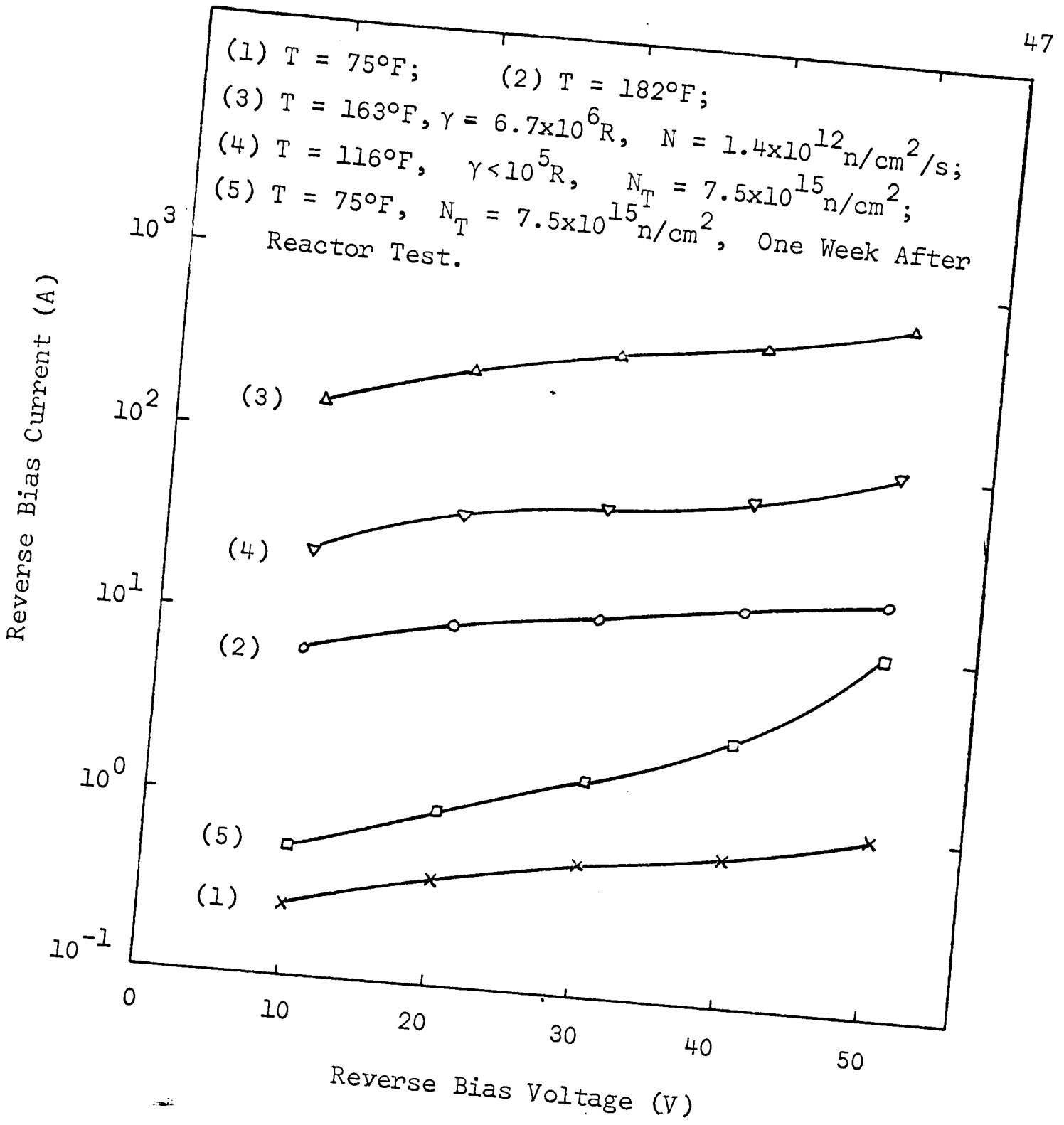

Figure 3.1. Reverse I-V characteristics in pre-avalanching region of passivated IMPATT diode. (After Anderson.[34])

structures with an active area of 10^{-4} cm^2. The n-region had a width of 4.5 microns and a doping concentration of 5×10^{15} cm^{-3}. Chaffin showed in his report that the diodes stopped oscillating during the radiation pulse, for both 7.0×10^7 rads/sec and 5.4×10^8 rads/sec dose rates but recovered almost immediately after the pulse. He indicated that the RF power came back to a slightly higher level after the pulse and then decayed to the original level within 1-2 msec. Chaffin attributed a decrease in diode voltage during the pulse to a decrease in breakdown voltage during the ionizing pulse. He explained the interruption in the oscillation by showing that the excess current density due to the electron-hole pair formation was greater than the normal reverse bias saturation current density. A large saturation current is expected to reduce the phase delay associated with the avalanche process and ultimately cause oscillations to cease if the negative conductance has become insufficient to overcome circuit losses.[33,46]

Borrego, et al,[47] measured the performance of double-epitaxial, diffused, and thermally grown oxide passivated diffused silicon IMPATT diodes under the influence of 100 nanosecond pulses of 10 MeV electrons at dose rates between 2×10^8 and 8×10^9 rad/sec. The RF performance of these 500 milliwatt, X-band diodes were tested in a tunable microwave cavity. The change in power at various fixed bias levels can be seen in Figs. 3.2, 3 and 4. The authors indicated that the diode power was reduced less than 50 percent for doses up to 10^9 rads/sec and was reduced to zero during radiation pulses for a dose rate of approximately 5×10^9 rads/sec. The typical value of external Q of

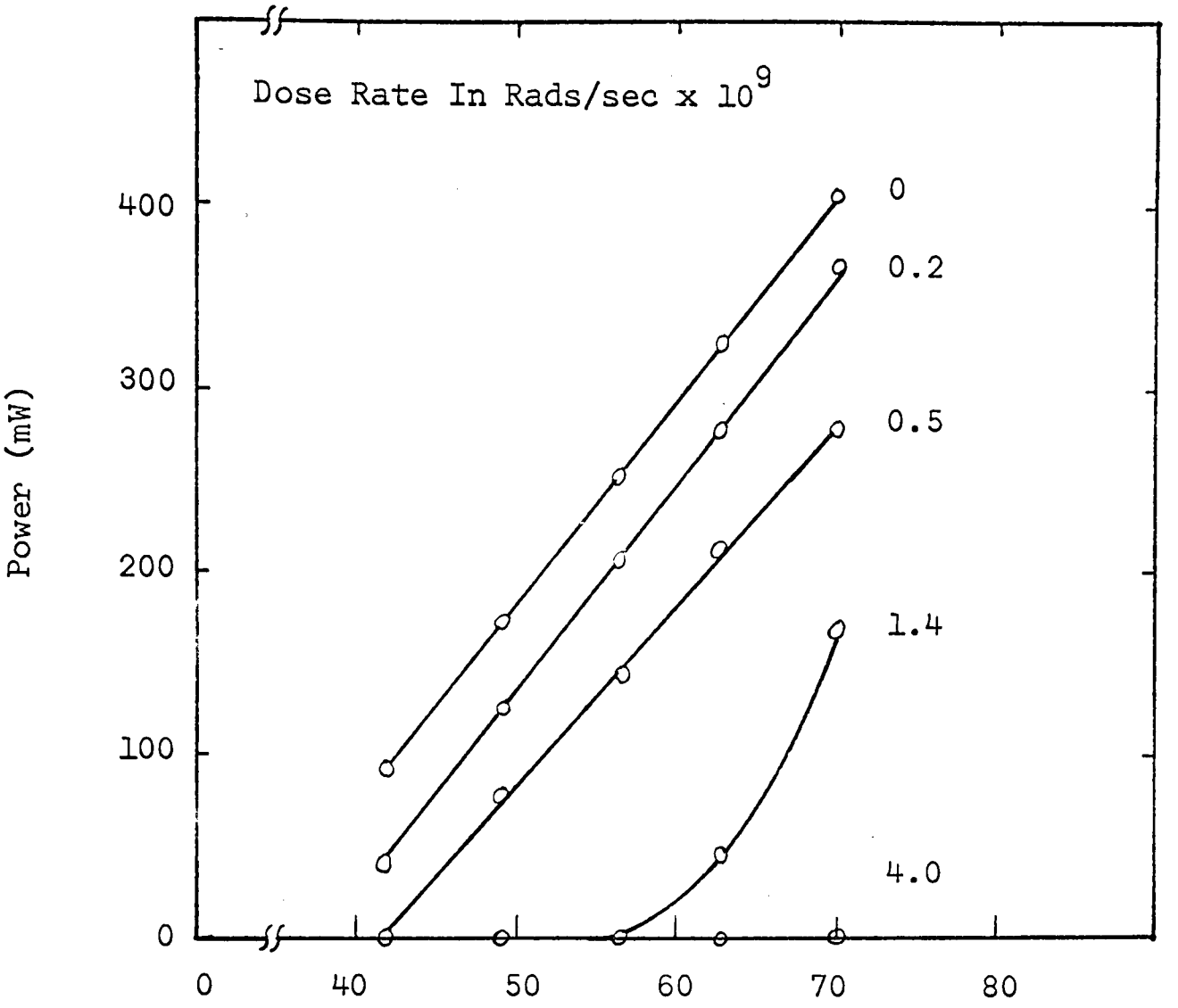

Figure 3.2. RF power during radiation pulse for double-epitaxial silicon diode in air filled, low Q cavity. (After Borrego, et al.[47])

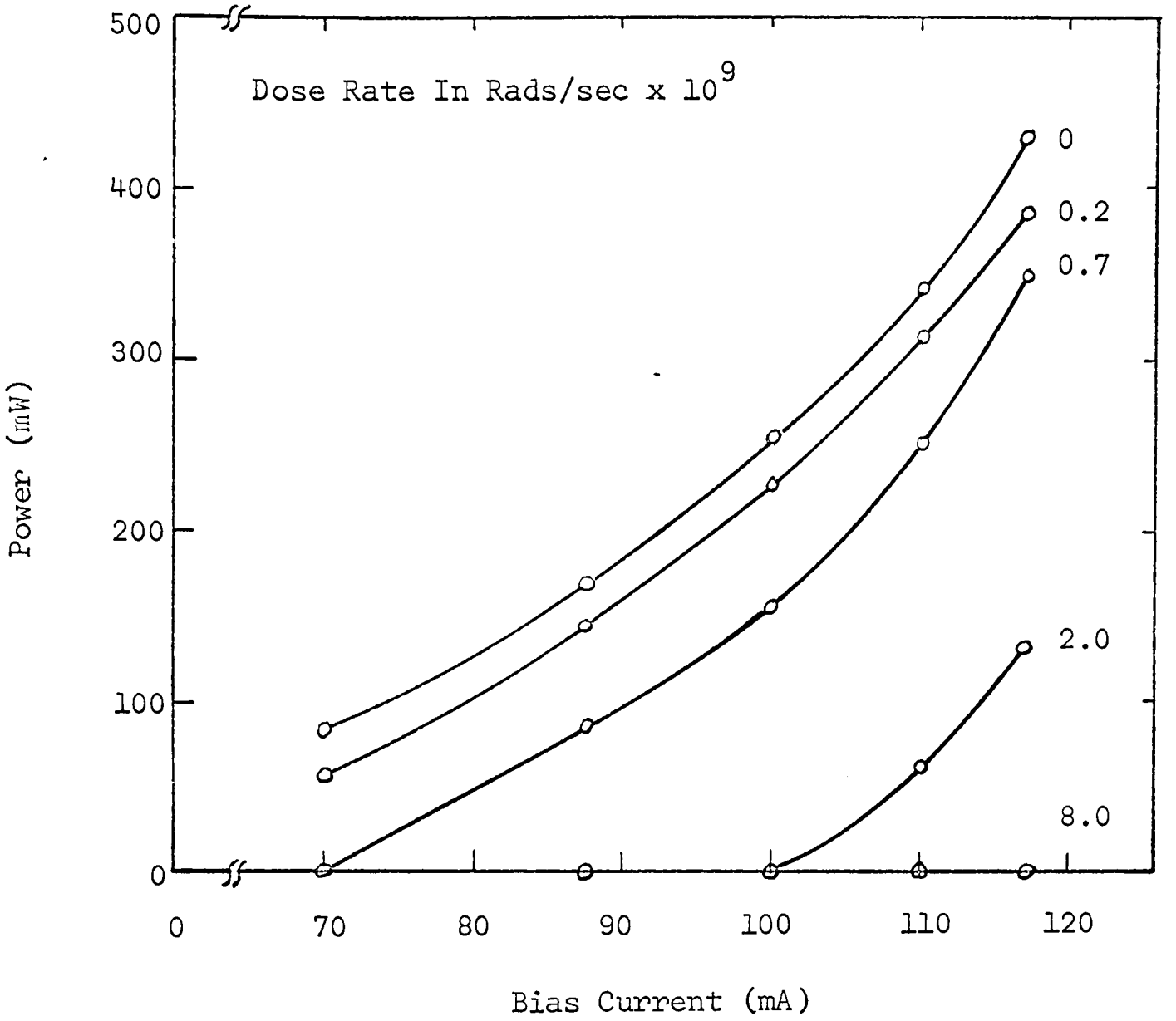

Figure 3.3. RF power during radiation pulse for diffused silicon diode in air filled, low Q cavity. (After Berrego, et al.[47])

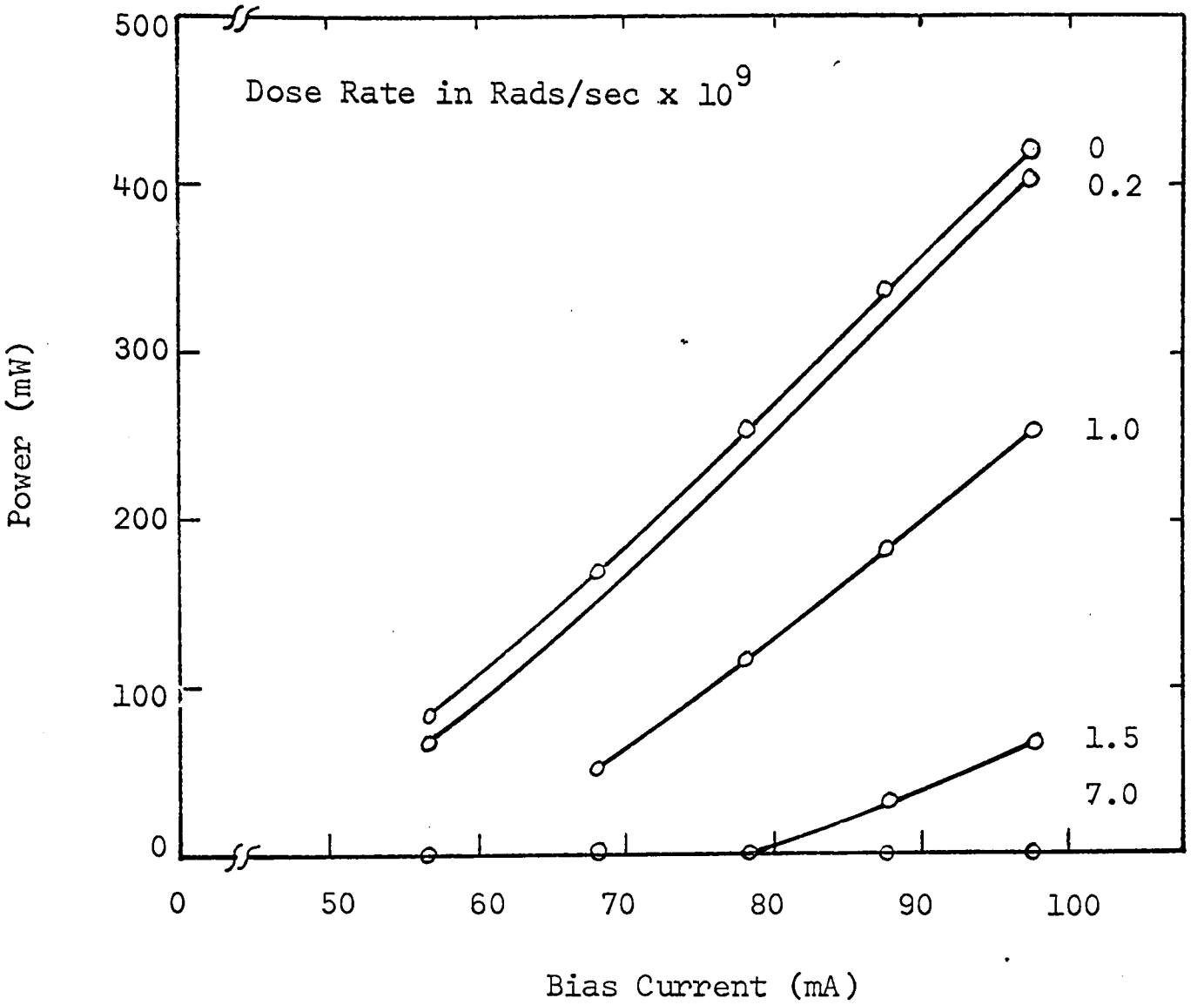

Figure 3.4. RF power during radiation pulse for diffused, thermally grown, oxide passivated, silicon diode in air filled, low Q cavity. (After Berrego, et al.[47])

the cavity was 100; however, the Q was increased to a value of 2000 for some experiments.[47] The frequency shifts for the diodes tested in the high Q cavity were lower than those obtained in the low Q cavity. The frequency shift for the three different types of diodes were similar with the results of the diffused diode shown in Fig. 3.5. They indicated that there was a time delay from 30-200 nanoseconds in the build up of RF power, in the high Q cavity, after the radiation pulse, which they attributed to the time necessary to build up oscillations in the cavity. They also indicated that the bias current of the diode did not change appreciably during the radiation pulse; however, bias voltage across the diode decreases due to an increase in leakage current.

The disagreement between investigators lies in the total gamma radiation required to quench IMPATT operations and the amount of elapsed time before oscillations would resume. While Anderson[30] reported that a neutron flux of 5×10^{15} n/cm^2 and a gamma flux of 5×10^{6} rads/sec caused IMPATT oscillations to stop for 15 minutes, Chaffin[33] reported that oscillations ceased at a total dose rate of 7×10^{7} rads/sec and resumed immediately after the radiation pulse. Borrego, et al,[47] later reported that oscillations in open air, low Q cavities were quenched when exposed to 10 MeV electrons at a dose rate of 9×10^{9} rads/sec.

B. LSA Devices

Experimental results published thus far pertaining to gamma radiation effects of gallium arsenide power devices have been concerned with Gunn and IMPATT diodes. The effects on the Gunn mode,

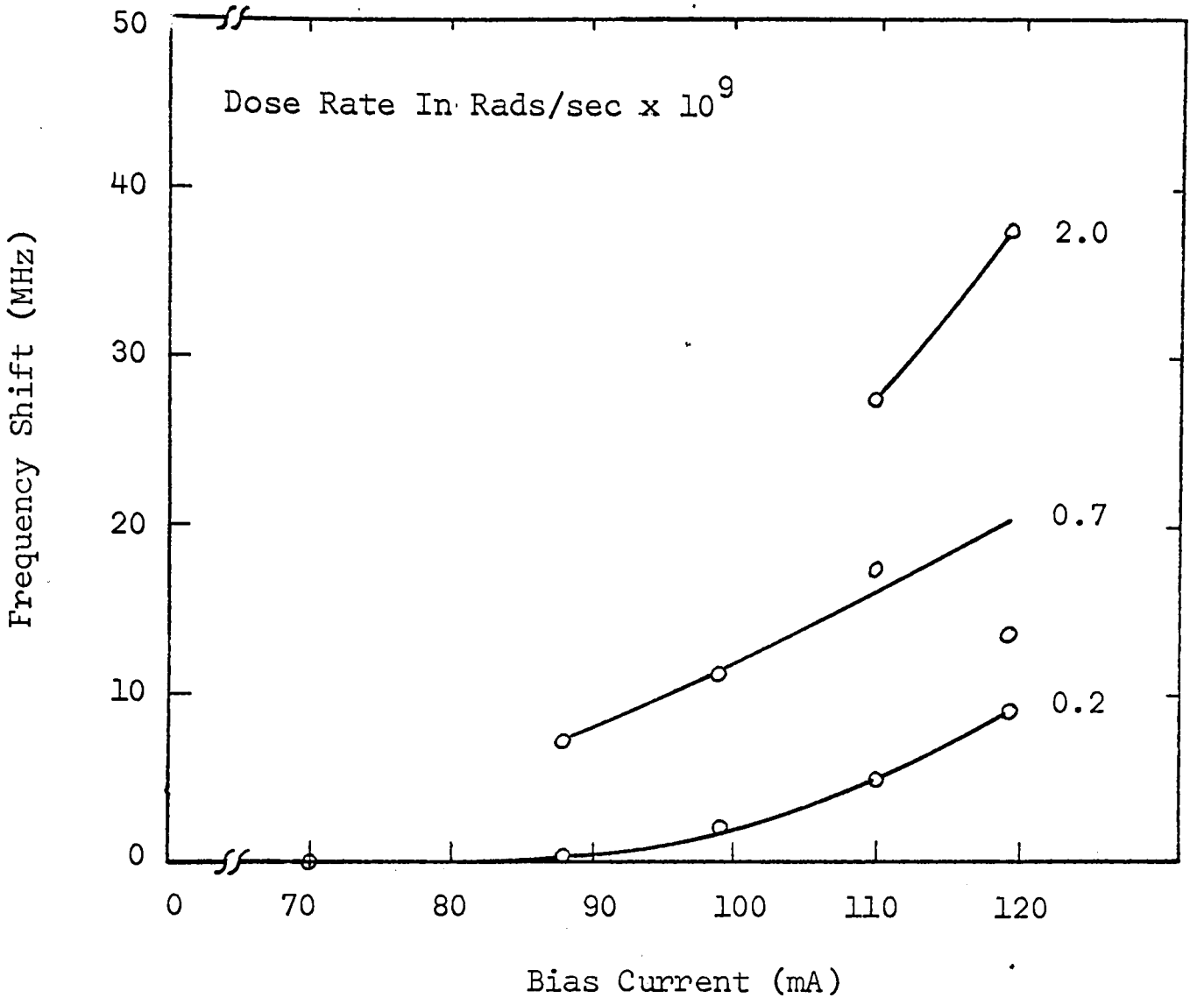

Figure 3.5. Frequency shift during radiation pulse for diffused, silicon diode in air filled, low Q cavity. (After Berrego, et al.[47])

however, provide useful information on the expected performance of LSA devices since the Gunn mode can be used to start the LSA oscillations. Copeland's[15] computer simulation results showed that the diode in a resonant circuit oscillated in the Gunn mode for about three cycles before the RF field was large enough to start the LSA oscillations. Other investigators,[48,49] however, have found it necessary to start the high power pulsed LSA diodes in the LSA mode of oscillation.

Anderson[50] performed measurements on an X-band Gunn diode under the influence of 2.1×10^6 rads of gamma radiation and found no significant change in frequency or I-V characteristics. He observed a very slight decrease in output power at higher power levels during irradiation and indicated that heat generation within the diode could have been the reason.

Chaffin[33] tested a 50 milliwatt, 10.5 GHz, CW Gunn oscillator operated at a current density of 1000 A/cm^2 under the influence of gamma radiation with dose rates as high as 5.4×10^8 rads/sec. The Gunn diode was a double-epitaxial gallium arsenide structure with an active area, length and doping of 4×10^{-4} cm^2, 1.2×10^{-3} cm and 8×10^{14} cm^{-3}, respectively. He found that the DC and RF parameters were unaffected at the dose rates employed in the test. The results were explained through his derivation of

$$\Delta n(t) = g_o T(1 - e^{-t/T}) \ , \qquad (3.7)$$

for the radiation generated carrier density, where g_o is the carrier generation rate conversion factor and T is the transit time (L/v_s) of the active region. Since Chaffin used a 40 μsec ionization pulse and the transit time was 1.2×10^{-10} (for $v_s \tilde{=} 10^7$ cm/sec for gallium

arsenide), t >> T and Eq. (3.7) reaches a steady-state solution of

$$\Delta n \tilde{=} g_o T \ . \qquad (3.8)$$

Equation (3.8) was used by Chaffin to show that the excess electrons generated for a dose rate of 7.0×10^7 rads/sec was three orders of magnitude lower than the doping concentration of the active region. Chaffin[51] indicated that it should take a dose rate of approximately 10^9 rads/sec to affect the diode, and that the effect should end within one transit time after the radiation pulse.

Berg and Dropkin[52] investigated the performance of both 100 milliwatt CW and 5 watt pulse mode 5 GHz Gunn diodes exposed to gamma radiation at dose rates between 10^8 and 5×10^{10} rads/sec. Both diodes were operated in a high Q coaxial cavity, and some measurements were also made on the pulse diodes operated in a resistive load (flat) cavity. It was found that a temporary cessation of power output in the high Q cavity and avalanche breakdown were the two failure modes for the Gunn diode oscillators exposed to the high intensity gamma radiation pulses. Berg and Dropkin concluded that the temporary cessation of power output was a result of the detuning and mode shifting of the diode oscillators in the high Q cavity caused by the excess carrier concentration and radiation induced photocurrents. The peak photocurrent (normalized to the Gunn threshold current) varied with total radiation dose in accordance with the curves plotted in Figs. 3.6 and 3.7. The investigators determined from the photocurrent data that the Gunn phenomenon was still present during radiation, and that the peak radiation induced carrier concentration can be found by

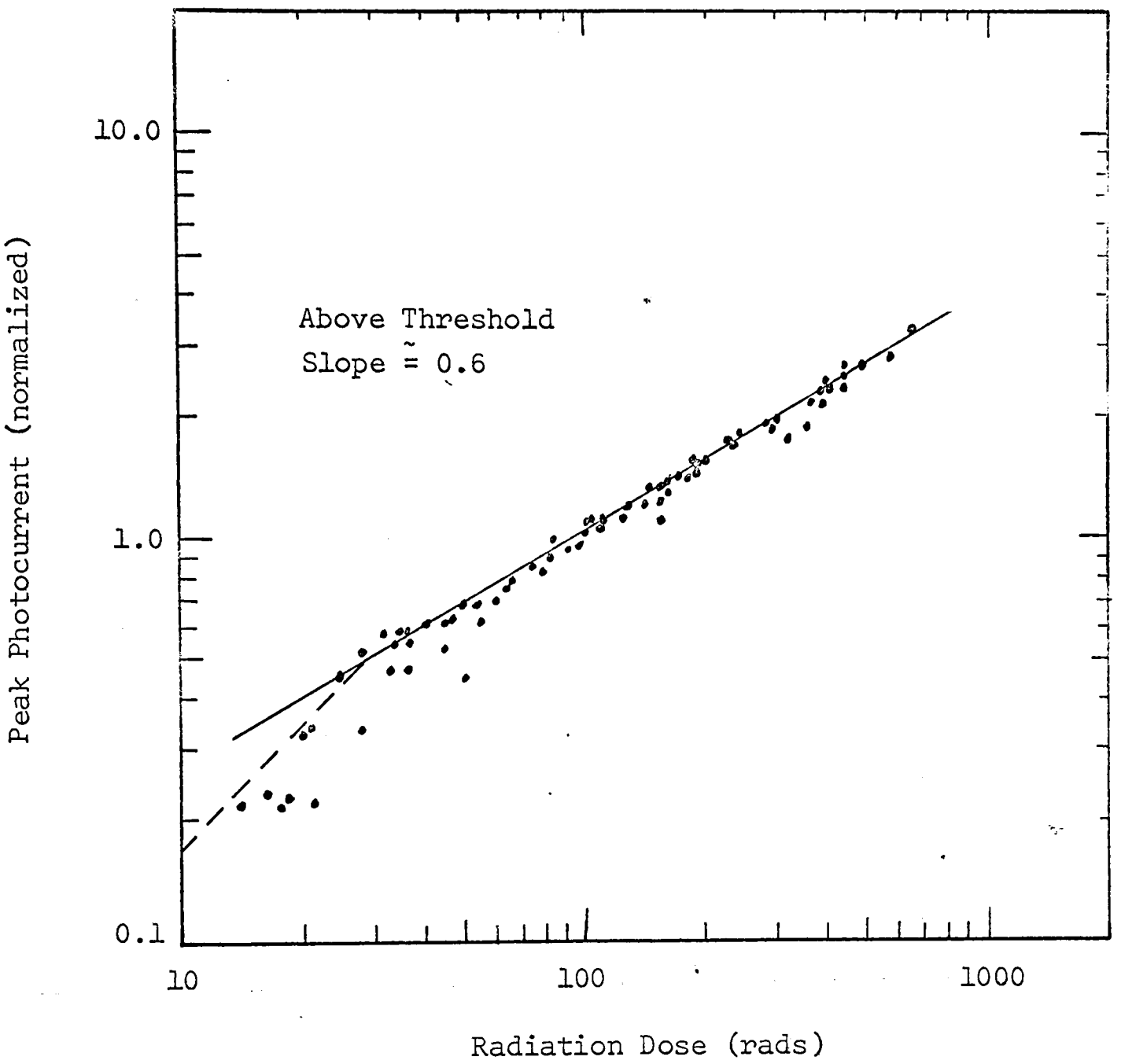

Figure 3.6. Normalized peak photocurrent versus radiation dose for both pulsed and CW diode oscillators. (After Berg and Dropkin.[52])

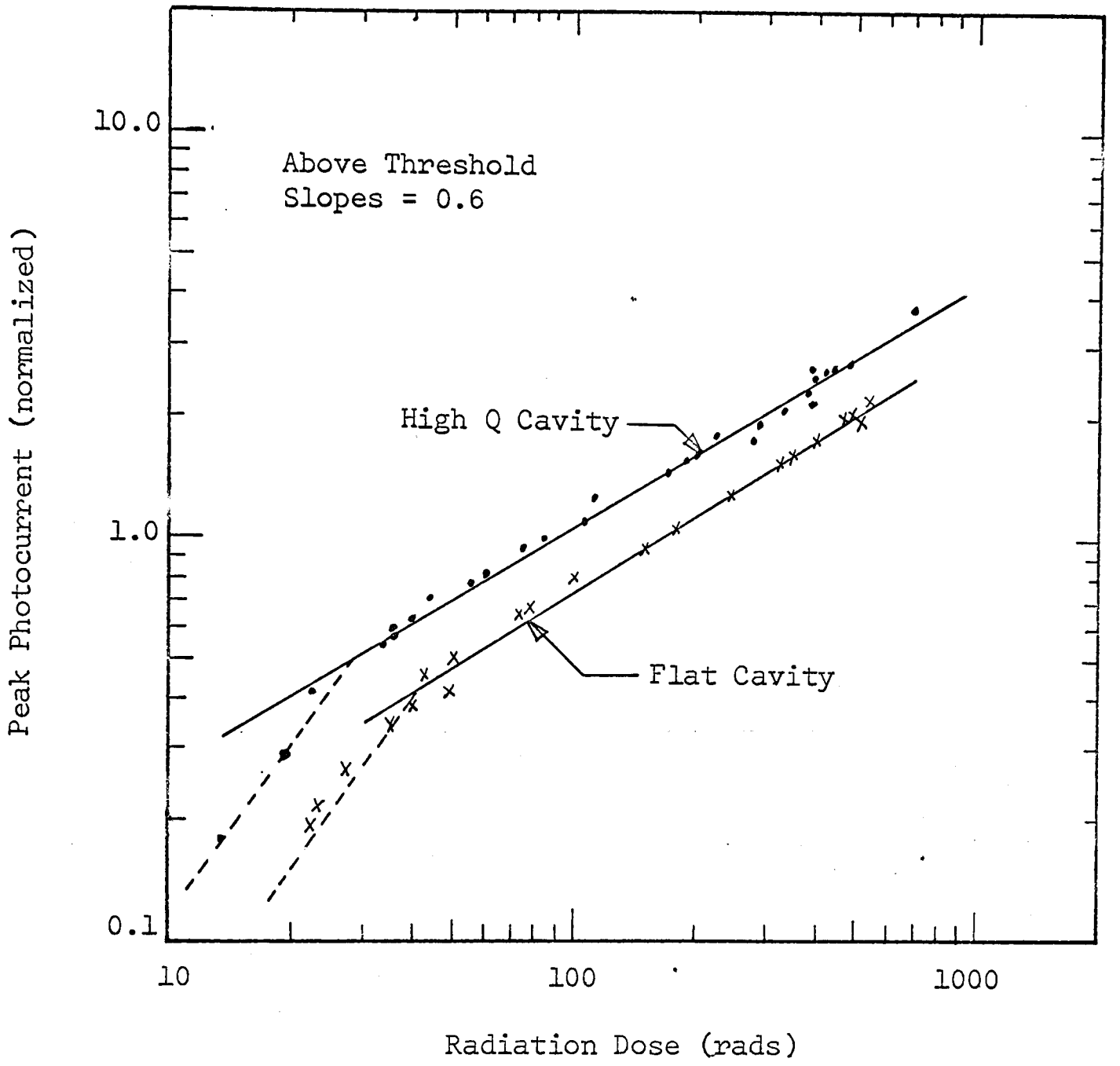

Figure 3.7. Normalized peak photocurrent versus radiation dose for both high Q and low Q cavity. (After Berg and Dropkin.[52])

$$n_{max} = 3 \times 10^{9}(\dot{\gamma})^{0.6} \text{ cm}^{-3} . \qquad (3.9)$$

Berg and Dropkin also observed that the temporary cessation of power output did not occur below 10^9 rads/sec whereas the effect first appeared at about 10^8 rads/sec for the CW diodes. Their results also indicated that once the output power was interrupted, a sharp recovery of output power occured in the high Q cavity oscillators while a more gradual recovery occured in the flat cavity device. There was a recovery time associated with the oscillators which depended upon the diode voltage and dose rate. Chaffin[51] has shown that the change in Q of the cavity and delay in recovery time due to ionization of the gas filling the cavity could be a possible explanation of this failure mode. Chaffin's results will be discussed later in this chapter. For the avalanche breakdown failure mode, Berg and Dropkin indicated that when the power output ceased the current increases to a large value and then decays at the end of the bias pulse. In some cases, the breakdown did not occur until after the end of the radiation pulse. It was also reflected that the avalanche failure mode appeared at the same radiation level for both cavities using pulsed diodes, and that CW diodes were not affected up to fluences of 5×10^{10} rads/sec. One of the explanations given by Berg and Dropkin was that the total carrier concentration was increased to such a high level (3 to 4 times larger than equilibrium concentration) that breakdown occured. This mechanism, however, did not explain some of their results. The other possible failure mechanism mentioned was that the radiation generated photocurrents increased the operating temperature of the diode to such a level that the negative resistance phenomenon was quenched, stopping

domain formation.

An increase in power in a Gunn device requires an increase in area; however, the power of an LSA device can be increased by increasing the device length.[13] The tendency in high power LSA devices is to have device lengths much greater than for Gunn devices. An increase in device length, increases the device transit-time resulting in an increase in the radiation generated carrier density using Eq. (3.8). This can be seen by comparing the radiation induced carrier concentration of Chaffin's Gunn oscillator and the LSA relaxation oscillator investigated by Wilson and Gregory, discussed in Chapter II. It would require a gamma radiation exposure rate of approximately 9.2 x 10^{10} rads/sec to induce a radiation generated carrier density equal to the doping density of the Gunn diode. On the other hand, for the LSA device having a length of 0.008 cm, for the induced carrier concentration to be equal to the doping density, approximately 2.5 x 10^{10} rads/sec are required even though the doping concentration of the LSA device is greater than that for the Gunn diode. Large values of induced carrier concentration will change the doping/frequency relationship which may cause oscillator failure due to domain formation. It has also been reported[13] that the LSA mode can tolerate only a smaller temperature rise inside the diode than other less sensitive modes of gallium arsenide devices. This is a result of the LSA mode being sensitive to resistivity gradients.

C. Device Configuration

Chaffin studied the effects of ionizing radiation on gas filled microwave cavities and found that ionization effects can not be

neglected above dose rates of 10^8 rads/sec.[51] His theoretical calculations reflected that a 45 percent decrease in the cavity Q would result from a dose rate of 4.8×10^8 rads/sec for 25 nsec due to ionization of the gas filling the cavity. Chaffin's experimental data indicated, also, that the period of disturbance increased with increasing dose rate.

Borrego, et al,[47] evaluated the power reduction of the double-epitaxial, silicon IMPATT oscillator mentioned earlier resulting from ionization of the air in the microwave cavity. The change in power at fixed bias currents due to increasing dose rates for the IMPATT diode operated in a low Q cavity in vacuum is shown in Fig. 3.8. These curves can be compared with those shown in Fig. 3.2 for the same diode operated in an air filled low Q cavity. The investigators indicated that the power output was affected by air ionization at dose rates larger than 3×10^9 rads/sec. The Q of the cavity changed 30 percent when exposed to a 100 nsec pulse of radiation at a dose rate of 3×10^9 rads/sec. Borrego, et al, also observed a delay (approximately 50 nsec) in the build up of RF power after the radiation pulse and attributed the delay to air ionization-recombination effects.

Alumina, sapphire and reinforced teflon substrates used in microstrip and stripline microwave circuits have been investigated by Wilson and Chaffin[42] to determine the effects from gamma radiation. Their results reflected no change in the microwave properties of the sapphire or alumina substrates at radiation doses as large as 1.3×10^8 rads(H_2O).* There was a slight discoloration of the alumina

---

*One rad in this context is the amount of radiation required to deposit 100 ergs/gm in H_2O.

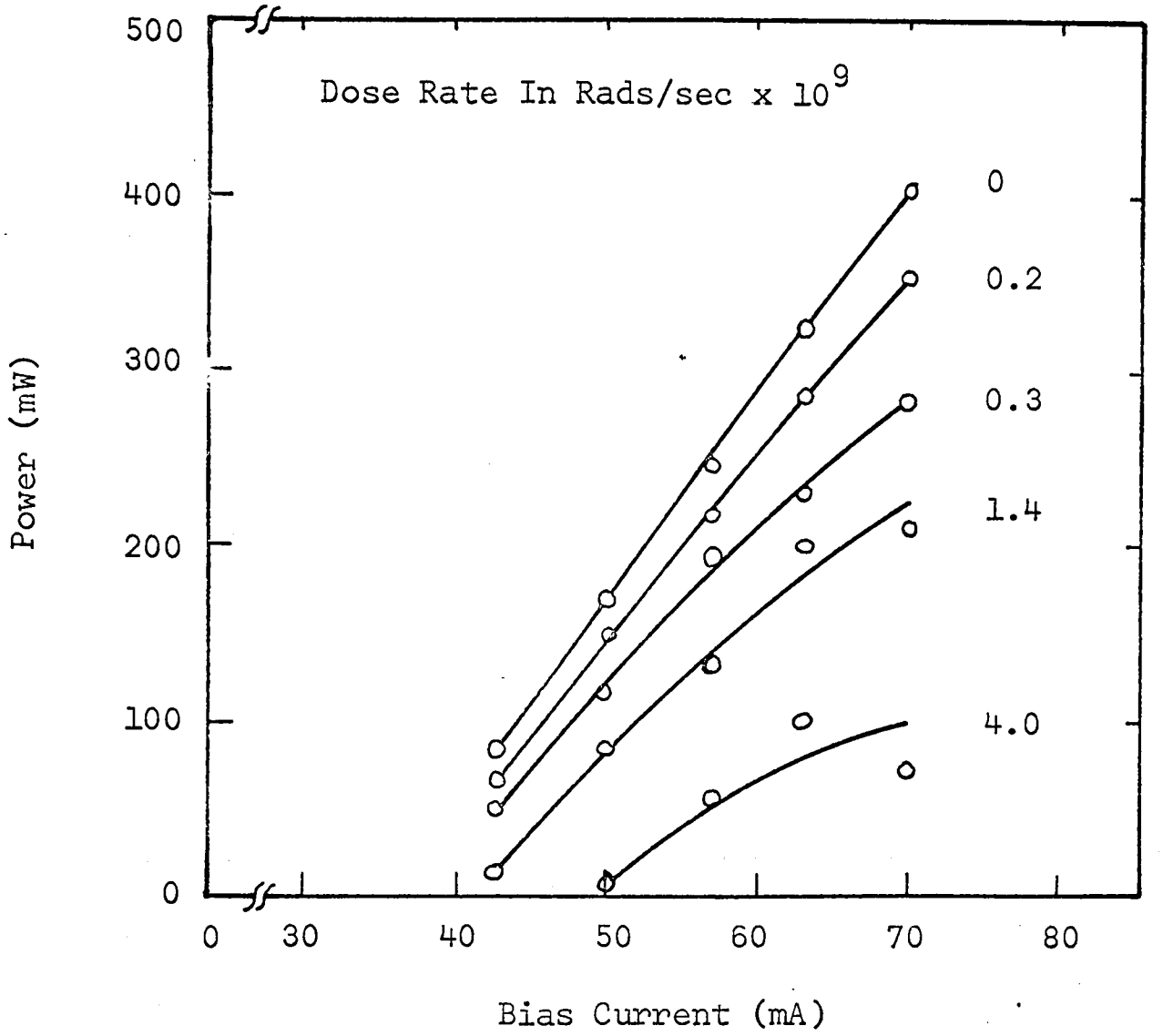

Figure 3.8. RF power during radiation pulse for double-epitaxial silicon diode in evacuated, low Q cavity. (After Borrego, et al.[47])

substrates, however, at gamma doses as low as 10^4 rads. The fiberglass reinforced teflon showed a gradual increase in dielectric constant and loss tangent.[42] The change in resonant frequency and unloaded Q of the microstrip bandpass resonant filter circuit constructed from teflon-glass substrates can be seen in Fig. 3.9.

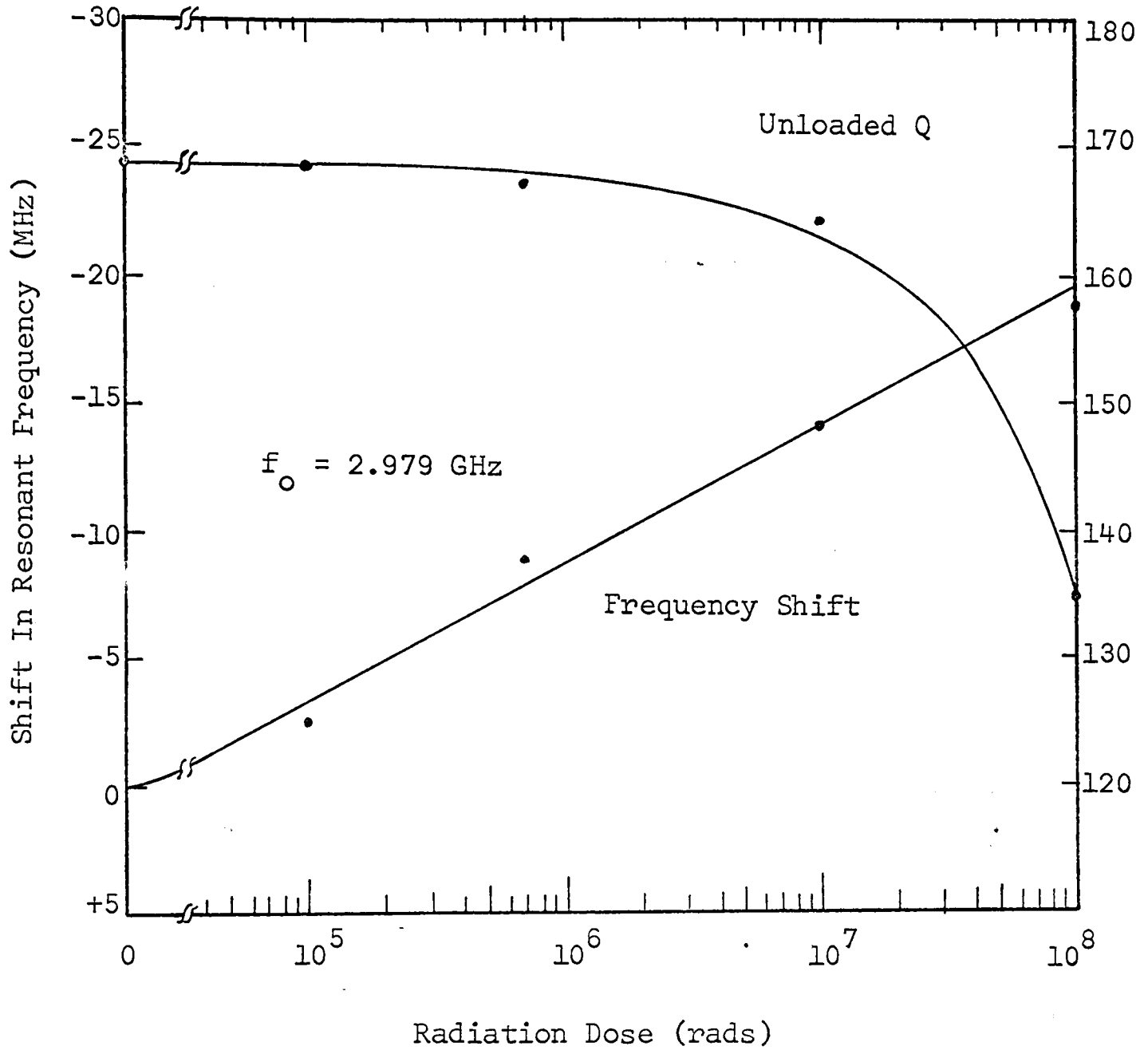

Figure 3.9. Change in resonant frequency and unloaded Q versus gamma radiation for microstrip resonator filter circuit composed of a teflon-glass substrate. (After Wilson and Chaffin.[42])

CHAPTER IV

CONCLUSIONS

The effects of nuclear radiation on the TRAPATT and LSA devices were discussed in Chapters II and III. Theory and experimental results have shown that the TRAPATT device is extremely tolerant to neutron exposure and can withstand fluences of one to two orders of magnitude greater than comparable LSA devices. Although insufficient experimental data exists concerning gamma radiation effects on these devices, the tolerance of TRAPATT devices should be fairly good. It has been shown that stripline and microstrip circuits composed of alumina or sapphire substrates are extremely resistant to radiation.

A. TRAPATT Devices

Results of the measurements indicated that little change in the RF parameters of TRAPATT oscillators for exposure levels as high as 10^{15} n/cm^2 can be expected. A reduction in the IMPATT oscillations is the ultimate RF failure mode of TRAPATT devices. This reduction in growth rate is a result of some carriers, injected by the avalanche process, recombining while transiting the space-charge region. A TRAPATT device will operate at a given frequency without serious degradation to average RF power output up to a fluence, ϕ, related to f by[35]

$$\phi = (0.33 \times 10^7)f \ , \qquad (4.1)$$

where ϕ is in units of neutrons per cm^2 (n/cm^2). This linear relationship, shown in Fig. 4.1, is not valid for fluence levels above approximately 10^{16} n/cm^2 due to the increased probability of DC thermal

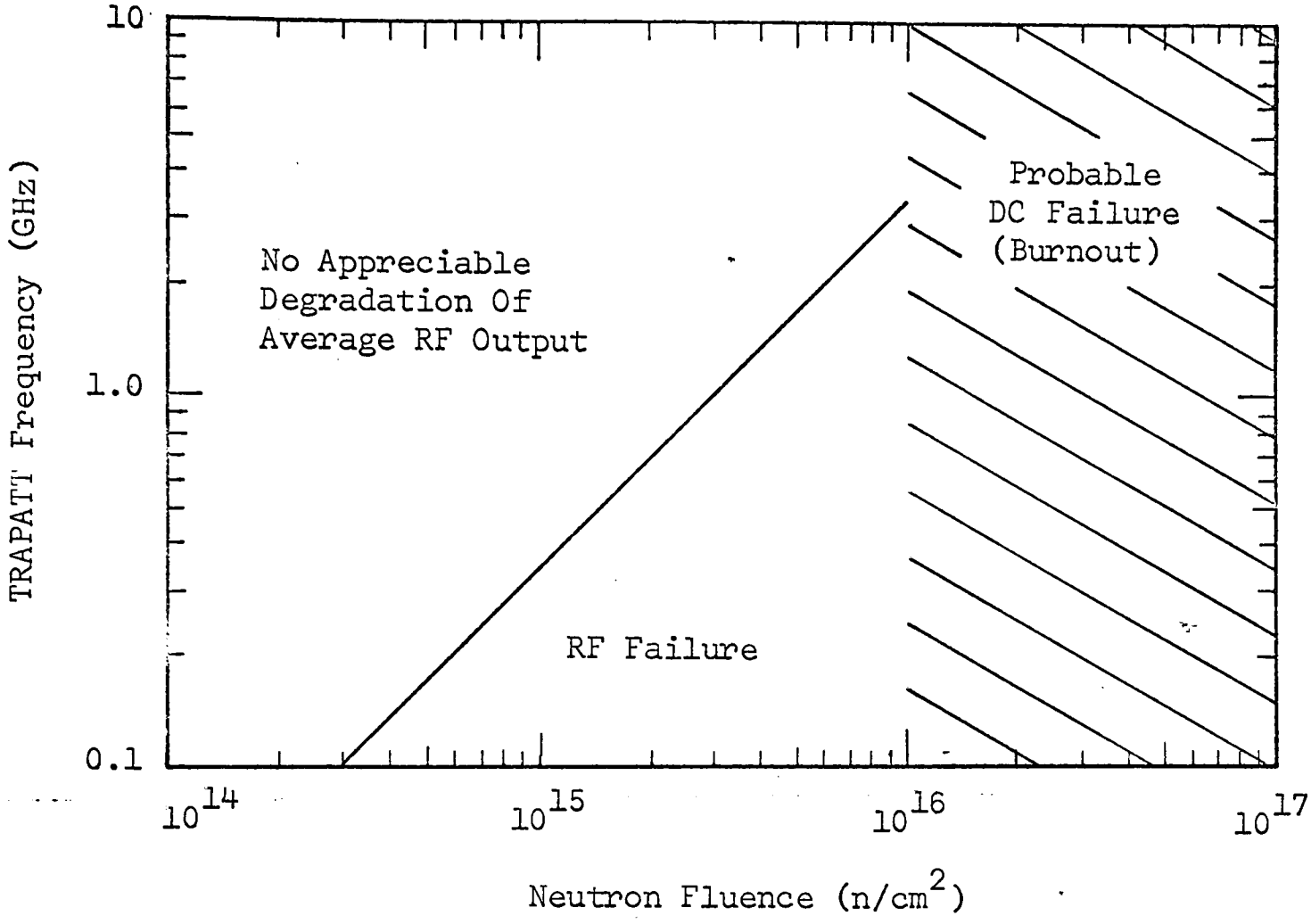

Figure 4.1. Graph outlining areas for no appreciable average RF output degradation, RF failure and for probably DC burnout. (After EerNisse and Chaffin.[35])

runaway caused by the negative temperature coefficient, $V^{-1}\ \partial V/\partial T$, effect. Carrier removal at the edges of the space-charge region, due to large fluences of neutron radiation, produces the negative temperature coefficient as well as an increase in breakdown voltage of the device. Devices with heavy doping in the p^+ and n^+ regions and with abrupt doping profiles will be more resistant than graded junction devices to carrier trapping at the edges of the space-charge region. The carrier recombination effect within the space-charge region caused by large neutron exposure levels can be reduced by using devices with shorter transit times. Shorter transit times, however, implies optimum shorter device widths, W, which are related to the frequency, f, of operation by[8]

$$W = 0.07\ v_{ns}/f\ , \tag{4.2}$$

where v_{ns} is the saturated electron drift velocity and has the value of $\backslash 10^7$ cm/sec for silicon structure devices. It can be seen from Eq. (4.2) that higher frequency devices will be more resistant to carrier recombination within the space-charge region due to a smaller optimum W. Higher frequency devices require higher doping densities in the active n region for proper device operation, and this also reduces the effect of carrier trapping in the n region. Carrier trapping in the active region localizes the avalanche zone near the p^+n side of the device and results in a slight pulling of the operating frequency with increasing neutron fluence. A general design criteria would indicate that hardened devices should be designed with higher carrier concentrations than normal.

There are a range of values for the doping density and bias

current which will allow TRAPATT oscillations. Clorfeine[53] developed a design triangle, in the j_{dc} - $N_D W$ plane, from which a designer could choose an operating point dependent upon the specific objectives of the device and obtain near optimum efficiencies. The hypotenuse is a curve, rather than a straight line, and represents those points where premature avalanche may occur. Premature avalanche can occur if the electric field across the junction rises to its avalanching value E_B before the plasma developed by the preceding avalanche has been removed.[53] Clorfeine indicated that premature avalanche can be avoided if

$$j_{dc} < \frac{r}{2} \left[(1 + r') \frac{\epsilon E_B}{qN_D W} - 1 \right] , \qquad (4.3)$$

where r is the ratio of hole-to-electron saturation velocities, r' is the ratio of hole-to-electron low field mobilities, $j_{dc} = J/2qv_{ns}N_D$), J is the total current density during plasma formation and extraction, $q = 1.6 \times 10^{-19}$ coulombs, and N_D is the doping density of the active region. It was reflected that E_B is a weak function of N_D and varies from 3.0×10^5 V/cm at 10^{15} cm^{-3} to 4.0×10^5 at 10^{16} cm^{-3} for silicon. Clorfeine's design triangle for an L-band, silicon structure device is shown in Fig. 4.2 with Eq. (4.3) plotted for values of r = 1, r' = 0.377, and $E_B = 3.0 \times 10^5$. The dotted curve is a plot of Eq. (4.3) taking $E_B = 4.0 \times 10^5$ which is appropriate for X-band oscillators. The $N_D W = \epsilon E_B/q$ line defines the condition in which avalanche occurs at the same voltage as that required for punch-through. The relative position of the triangle with this line indicates that the electric field in a properly designed device will punch through to the n^+ region well

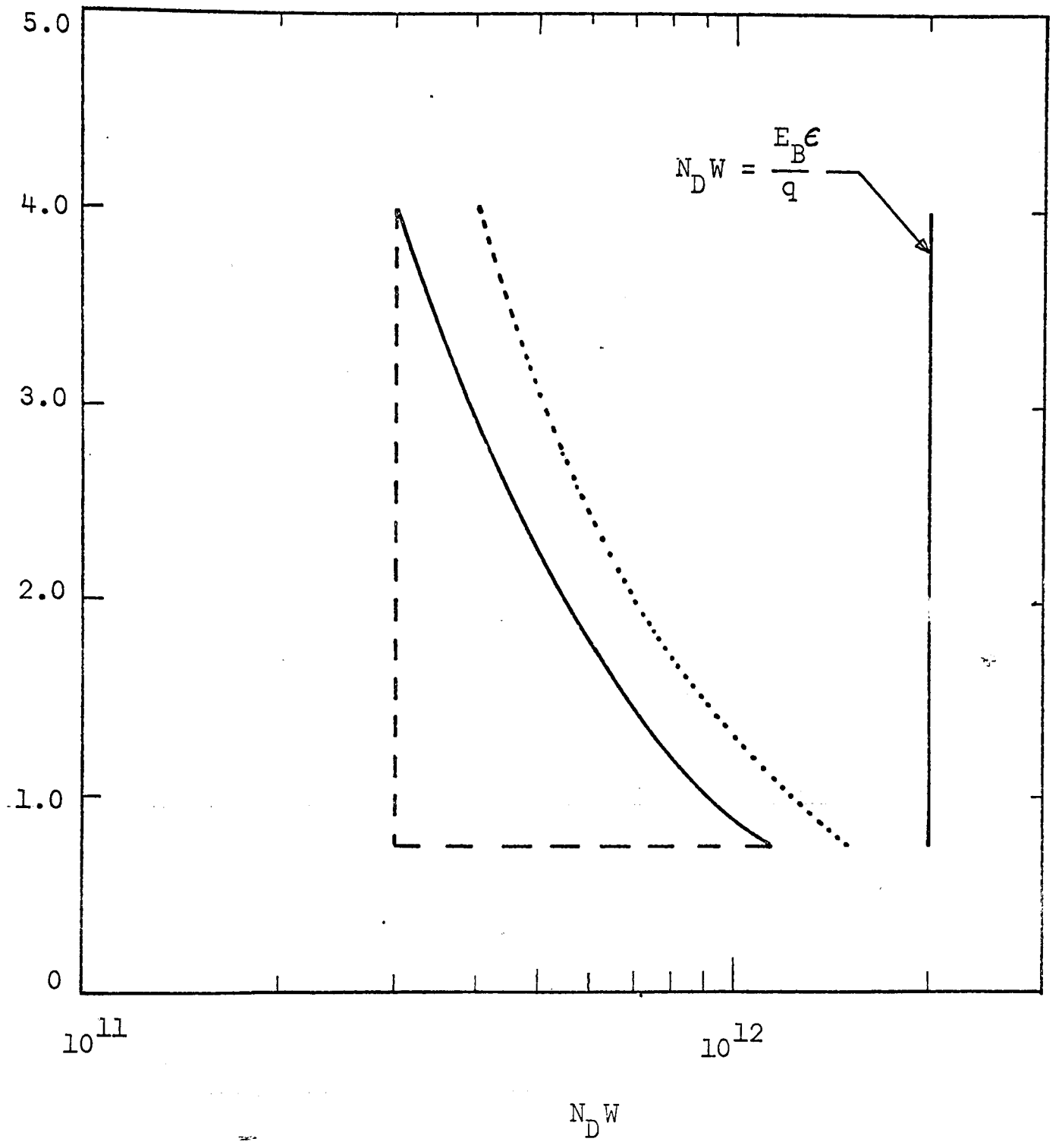

Figure 4.2. TRAPATT design triangle. (After Clorfeine.[53])

before breakdown. One side of the triangle is formed by $j_{dc} = 0.75$ since higher efficiencies are expected at higher current densities. The other side of the triangle, resulting in a lower limit for the $N_D W$ product, is not well defined and is emphasized by the gray area in Fig. 4.2. The uncertainty in choosing this lower limit may depend on several circumstances, one of which is possible difficulties in fabricating diodes with low doping densities and high current carrying capacities. Clorfeine chose $N_D W = 4.0 \times 10^{11}$ cm^{-2} as the lower limit. The triangle can be used as a guide in choosing an operating point and should provide near optimum efficiencies. The operating point selected, however, will normally depend on whether the diode will be used for CW, high efficiency or high pulse power operations. Clorfeine showed that the maximum RF power per unit area is obtained in the upper left-hand corner of the triangle and should be desirable for low-duty cycle pulse operation where device heating is not a major problem. He also showed that the lower left-hand corner of the triangle was most desirable for CW operation in which there is a need to minimize per unit area dissipated power and still maintain high efficiencies.

In designing a diode to operate in a nuclear weapons environment, the most suitable operating point would probably be in the center of the design triangle. This location will permit small decreases in the $N_D W$ product and j_{dc} due to carrier removal caused from neutron radiation and still provide for high efficiency operation. This operating point also permits small increases in these same values due to gamma radiation-induced carrier concentration without premature avalanche

occurring. The exact operating point selected, however, would depend upon the extent of the fluence levels in which the device must continue to operate.

One of the primary effects of changing temperature is a decrease in ionization coefficient as the diode temperature increases, resulting in a higher breakdown voltage. Increasing temperature also decreases the carrier velocity resulting in a decrease in current density and device frequency. Matsumura[54] has indicated that an abrupt type diode junction is more resistant to thermal effects. The change in frequency and power with increasing temperature for an L-band TRAPATT oscillator is shown in Fig. 4.3. Adjustments can be made in the applied bias, however, to provide essentially constant frequency and power characteristics as long as the device temperature remains below approximately 150° to 200°C to prevent thermal instabilities.[55] It has also been stated that non-passivated diodes are more resistant to radiation exposure than passivated ones.

B. LSA Devices

Results of measurements on high peak-power LSA diode oscillators indicated that the RF parameters began to change at neutron fluence levels of approximately 10^{13} n/cm^2. The primary cause of LSA diode failure, from large levels of neutron fluence, is from an increase in low field resistance which results in an increase in device frequency and a reduction in breakdown voltage. Additionally, there is a reduction in current after heavy irradiation which is probably due to carrier trapping. The experimental results also reflect that the frequency change, due to neutron exposure, limits the use of the LSA

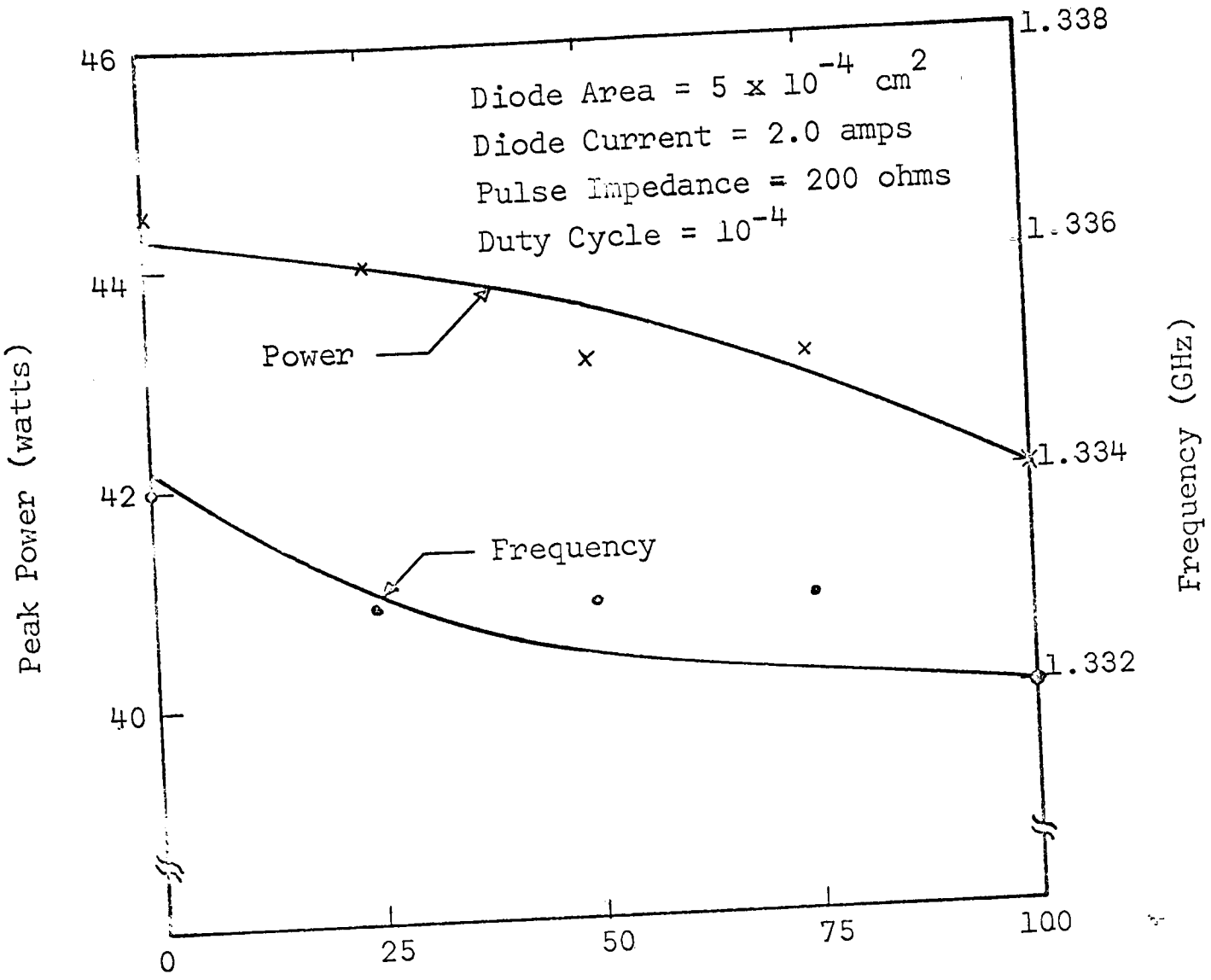

Figure 4.3. Behavior of TRAPATT oscillator power and frequency with changing temperature. (After Wilson.[45])

device before other radiation problems, due primarily to reduced mobility. Highly doped devices would be harder because of the larger fluence levels required for given change in low field resistance. Fluences on the order of 10^{14} n/cm^2, however, is the upper limit for X-band oscillators.

In designing LSA devices, the carrier concentration in the active region is primarily determined by the frequency of operation of the device, and for n-type gallium arsenide at room temperature, the ratio of doping to frequency (N_D/f) should be in the range

$$2 \times 10^4 < N_D/f < 2 \times 10^5 \text{ sec/cm}^2 . \qquad (4.4)$$

The doping to frequency ratio is normally about 1×10^5 sec/cm^3. LSA diodes also have a doping to active layer length, N_DL, of $N_DL > 1 \times 10^{13}$ cm^{-2}. The relationship between the LSA mode and other modes of operation using gallium arsenide is shown in Fig. 4.4. In a nuclear radiation environment, however, the active layer length should be reduced in order to make the device transit time as small as possible. A reduction in power will accompany a decrease in device length.

In high quality gallium arsenide epitaxial diodes, an increase in temperature has very little effect on the carrier concentration; however, the mobility decreases causing an increase in low field resistance. The increase in frequency and decrease in power which follows the increase in temperature can be seen in Fig. 4.5. The device thermal impedance should be kept as small as possible to minimize the average temperature rise of the active region, since temperature increases cause a reduction in the rates of threshold to saturated (peak/valley) carrier velocities which is the determining factor for

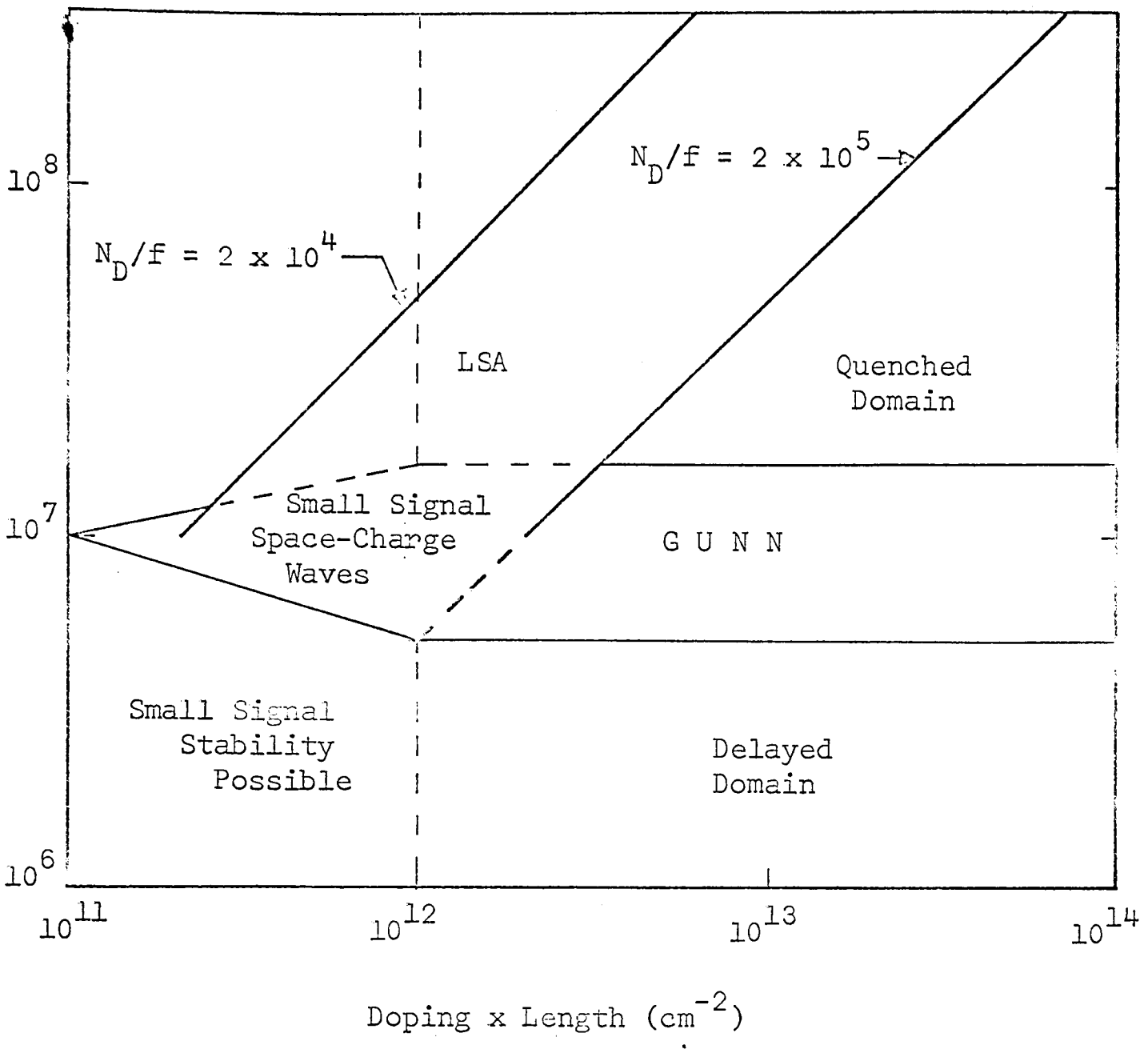

Figure 4.4. LSA mode in relation to other modes of gallium arsenide diodes in terms of frequency x length and doping x length. (After Copeland.[15])

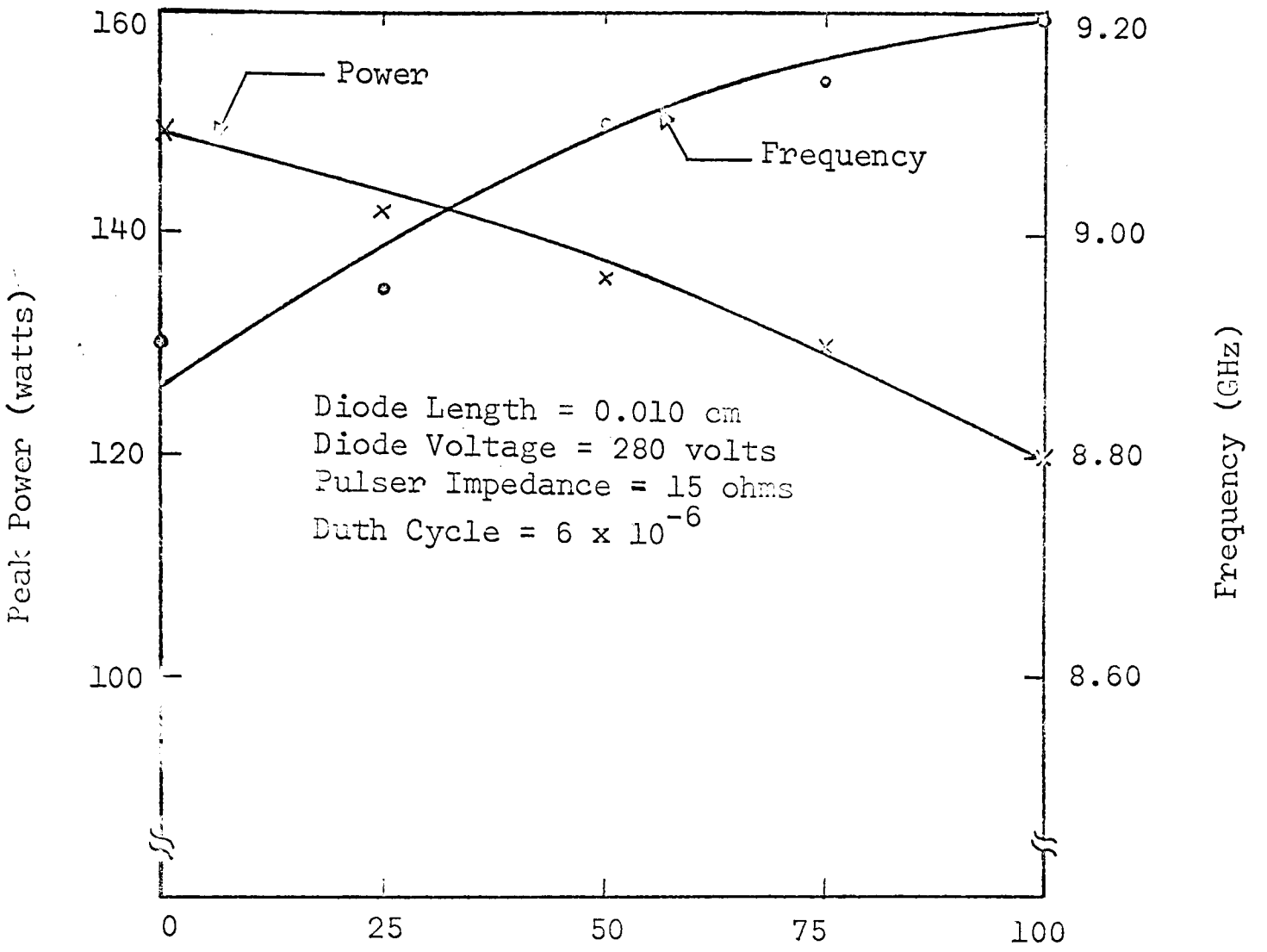

Figure 4.5. Behavior of LSA oscillator power and frequency with changing temperature. (After Wilson.[45])

device efficiency.

The electron concentration in bulk grown n-type gallium arsenide is strongly temperature dependent due to the oxygen compensation used to allow large doping levels and can lead to thermal distruction. The increased carrier density caused from ohmic heating allows a domain to fully form ($N_D/f > 2 \times 10^5$) and can result in avalanche. The LSA mode of operation will fail due to domain formation, even if thermal instabilities are not great enough to cause device destruction. Device destruction can result when the temperature is increased to such a level that the contacts melt or when the peak to valley ratio is reduced to 1. Temperature effects are more critical in the LSA mode of operation than in other devices or modes due to the poor thermal conductivity of gallium arsenide.

C. Thermal Dissipation

The performance of the TRAPATT and LSA devices is limited by thermal effects--even in a non-nuclear environment. One of the major problems faced by the device designer will, therefore, be that of heat transfer from the diode. Even though the maximum operating temperature of silicon is less than gallium arsenide, the thermal constraints of the silicon TRAPATT devices are less severe than those for the gallium arsenide LSA devices since silicon has the highest thermal conductivity and most of the heat is generated in the p^+n junction where the major portion of the avalanche occurs.

The procedure normally used for effective heat dissipation consists of flip-chip mounting, where as an example, the p^+ end of the p^+nn^+ TRAPATT diode is in contact with the heat sink. A good thermal

contact is obtained by diffusion welding between two gold layers. The bonding mechanism in diffusion welding is the exchange of atomic sites between similar metals.[56] The direct metal plating of the heat sink to the diode is another method of lowering the thermal contact resistance.[57] Clorfeine[53] calculated the allowable power dissipation consistent with a maximum temperature of 200°C inside the diode. The results are shown in Fig. 4.6 for both copper and type IIA diamond. He assumed 5μ regions of p^+ and n, with the far ends of the heat sink maintained at 25°C. Clorfeine further indicated that higher power levels could be predicted if two sided heat sinking or cooling were employed. The second heat sink increases the dissipation rating by a factor of two for large diameter diodes where the heat sinks themselves are the chief contributors to the thermal resistance, and by a factor of four for diodes in which the active region presents the major resistance.[58] For gallium arsenide devices, the heat sink bonding technique which can be used is by essentially soldering the chip with a thin layer of AuGe.[59] Surface oxides are eliminated by using a chemical flux.[59]

Theory and experimental results have shown that TRAPATT devices are more desirable than comparable LSA devices for operations in a nuclear weapons environment. For both the TRAPATT and LSA modes, higher operating frequencies will yield harder devices due to the higher doping levels required. There is a lack of experimental data concerning gamma radiation effects on both devices and warrants further investigation before a complete analysis of these effects can be made. Theory reflects that the gamma radiation tolerance of both

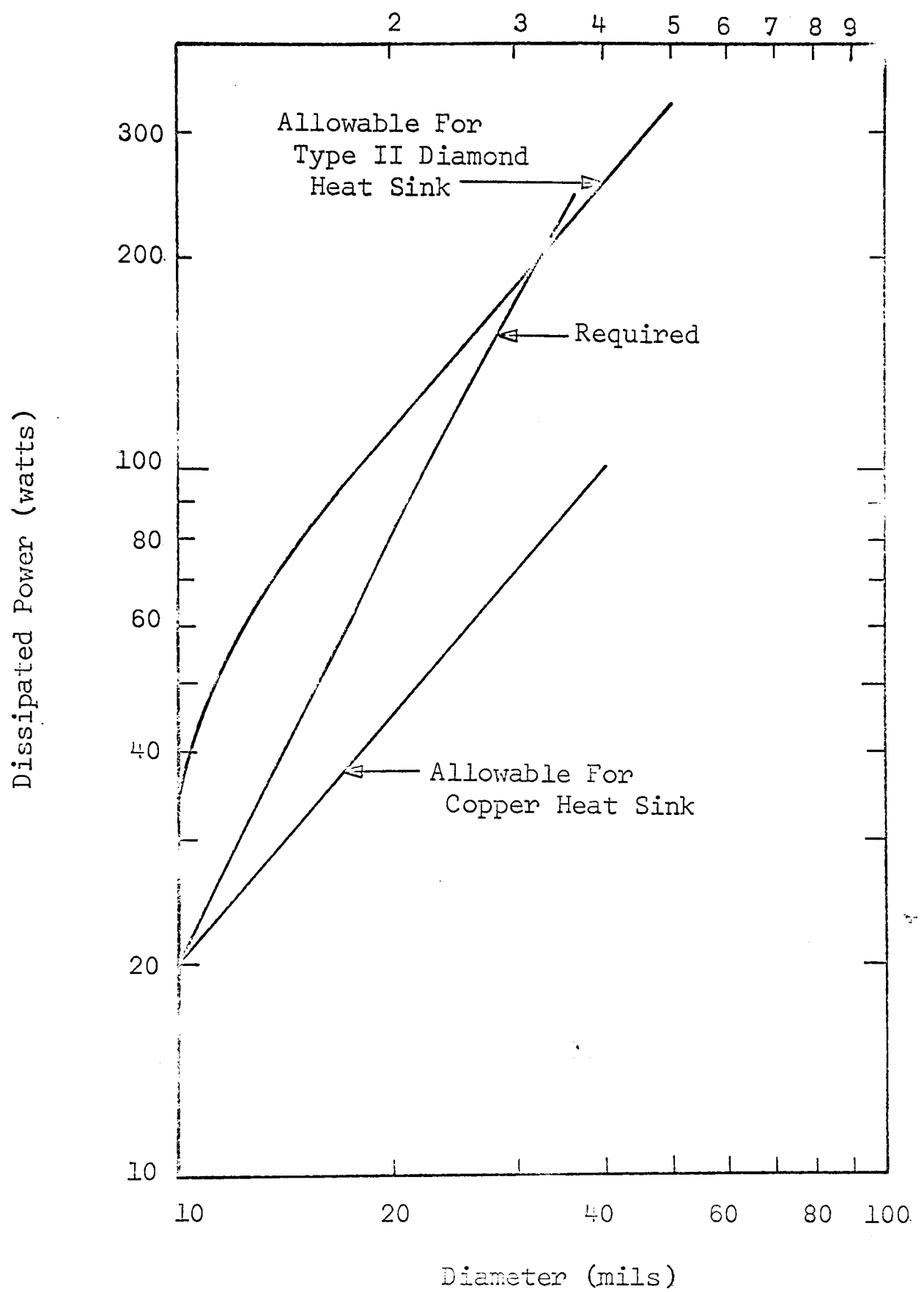

Figure 4.6. Thermal limitations in TRAPATT oscillators. (After Clorfeine.[53])

TRAPATT and LSA devices should be fairly good with shorter active region diodes yielding harder devices.

LIST OF REFERENCES

1. Poll, R.A., "Approaches to System Hardening," IEEE Trans. Nucl. Sci., Vol. NS-17, December 1970, pp. 83-90.

2. Spratt, J.P., Schnable, G.L., and Standeven, J.D., "Impact of the Radiation Environment on Integrated-Circuit Technology," IEEE J. Solid-State Circuits, Vol. SC-5, February 1970, pp. 14-24.

3. Kalinowski, J.J., and Thatcher, R.K., (Editors), TREE Handbook, Battelle Memorial Institute, DASA 1420, September 1969.

4. Larin, F., Radiation Effects in Semiconductor Devices, John Wiley and Sons, New York, 1969.

5. van Lint, V.A.J., Mechanisms of Transient Radiation Effect, Gulf General Atomic, Inc., GA-8810, August 1968.

6. Wilson, W.E., "Pulsed LSA and TRAPATT Sources for Microwave Systems," Microwave Journal, Vol. 14, August 1971, pp. 33-41.

7. Prager, H.J., Chang, K.K.N., and Weisbrod, S., "High-power, High Efficiency Silicon Avalanche Diodes at Ultrahigh Frequencies," Proc. IEEE (Lett.), Vol. 55, April 1967, pp. 586-587.

8. Clorfeine, A.S., Ikola, R.J., and Napoli, L.S., "A Theory for the High Efficiency Mode of Oscillation in Avalanche Diodes," RCA Review, Vol. 30, September 1969, pp. 397-421.

9. DeLoach, B.C. and Scharfetter, D.L., "Device Physics of TRAPATT Oscillators," IEEE Trans. Electron Devices, Vol. ED-17, January 1970, pp. 9-21.

10. Wilson, W.E., TRAPATT Oscillator Sources: Design Principles and Experimental Circuits, Sandia Laboratories, SC-DR-71-0785, January 1972.

11. Haddad, G.I., Greiling, P.T., and Schroeder, W.E., "Basic Principles and Properties of Avalanche Transit-Time Devices," IEEE Trans. Microwave Theory Tech., Vol. MTT-18, November 1970, pp. 752-772.

12. Copeland, J.A., "A New Mode of Operation for Bulk Negative Resistance Oscillators," Proc. IEEE (Lett.), Vol. 54, October 1966, pp. 1479-1480.

13. Hershberger, W.D., (Editor), Topics In Solid State And Quantum Electronics, John Wiley and Sons, New York, 1972, pp. 20-98.

14. Watson, H.A., (Editor), Microwave Semiconductor Devices and Their Circuit Applications, McGraw-Hill Book Co., New York, 1969, pp. 497-536.

15. Copeland, J.A., "LSA Oscillator-Diode Theory," J. Appl. Phys., Vol. 38, July 1967, pp. 3096-3101.

16. Billington, D.S., and Crawford, J.H., Jr., Radiation Damage in Solids, Princeton University Press, New Jersey, 1961.

17. Olesen, H.L., Radiation Effects on Electronic Systems, Plenum Press, New York, 1966.

18. Crawford, J.H., Jr., and Cleland, J.W., "Nature of Bombardment Damage and Energy Levels in Semiconductors," J. Appl. Phys., Vol. 30, August 1959, pp. 1204-1213.

19. Gossick, B.R., "Disordered Regions in Semiconductors Bombarded by Fast Neutrons," J. Appl. Phys., Vol. 30, August 1959, pp. 1214-1218.

20. Gregory, B.L., "Minority Carrier Trapping by Defect Clusters," Appl. Phys. Letters, Vol. 16, January 1970, pp. 67-69.

21. Gregory, B.L., "Minority Carrier Recombination in Neutron Irradiated Silicon," IEEE Trans. Nucl. Sci., Vol. NS-16, December 1969, pp. 53-62.

22. Watkins, G.D., and Corbett, J.W., "Defects in Irradiated Silicon: Electron Paramagnetic Resonance of the Divacancy," Phys. Rev., Vol. 138, April 1965, pp. A543-A560.

23. Kalma, A.H., and Corelli, J.C., "Photoconductivity Studies of Defects in Silicon: Divacancy-Associated Energy Levels," Phys. Rev., Vol. 173, September 1968, pp. 734-745.

24. Wilson, D.K., "Capacitance Recovery in Neutron-Irradiated Silicon Diodes by Majority and Minority Carrier Trapping," IEEE Trans. Nucl. Sci., Vol. NS-15, December 1968, pp. 77-83.

25. Azarewicz, J.L., Research on the Physics of Transient Radiation Effects, Harry Diamond Laboratories, HDL-TR-060-3, February 1972.

26. Wilson, D.K., Lee, H.S., and Hoffke, H., "Radiation Effects on Silicon Avalanche (IMPATT) Diodes," IEEE Trans. Nucl. Sci., Vol. NS-15, December 1968, pp. 114-125.

27. Chaffin, R.J., "The Effect of Neutron Radiation on an IMPATT Diode," IEEE Trans. Microwave Theory and Tech., Vol. MTT-17, February 1969, pp. 119-120.

28. Anderson, W.A., "The Performance of IMPATT Diodes Under the Influence of High-Intensity Gamma and Neutron Radiation," Proc. IEEE (Lett.), Vol. 57, August 1969, pp. 1441-1442.

29. Chaffin, R.J., EerNisse, E.P., and Hood, J.A., "The Effect of Neutron Irradiation on the TRAPATT Diode," Proc. IEEE (Lett.), Vol. 57, November 1969, pp. 2063-2064.

30. Anderson, W.A., "A Radiation Pulse Interrupts IMPATT Diode Oscillation," Proc. IEEE (Lett.), Vol. 58, May 1970, p. 807.

31. EerNisse, E.P., "Temperature Coefficients of Avalanching p^+nn^+ Junctions With Carrier Trapping," Appl. Phys. Letters, Vol. 16, June 1970, pp. 506-508.

32. EerNisse, E.P., and Chaffin, R.J., "Carrier Trapping and Recombination in Avalanche Diodes," IEEE Trans. Electron Devices, Vol. ED-17, July 1970, pp. 520-526.

33. Chaffin, R.J., Transient and Permanent Radiation Effects in Gunn and IMPATT Oscillators, Sandia Laboratories, SC--RR-710378, June 1971.

34. Anderson, W.A., "Comparing Radiation Effects in Gunn and IMPATT Diodes," IEEE Trans. Nucl. Sci., Vol. NS-18, August 1971, pp. 404-409.

35. EerNisse, E.P., and Chaffin, R.J., "Design of Nuetron Radiation Tolerant High Efficiency Microwave Avalanche Diode Sources (TRAPATT Oscillators)" IEEE Trans. Nucl. Sci., Vol. NS-17, December 1970, pp. 227-229.

36. Buehler, M.G., "The Space-Charge Region of Neutron-Irradiated Silicon p^+n Junctions," IEEE Trans. Nucl. Sci., Vol. NS-17, December 1970, pp. 341-347.

37. Kimerling, L.C., and Drevinsky, P.J., "Carrier Removal Effects in Neutron-Irradiated Lithium-Doped Silicon," IEEE Trans. Nucl. Sci., Vol. NS-18, December 1971, pp. 60-68.

38. Berg, N., and Dropkin, H., "Neutron Displacement Effects in Epitaxial Gunn Diodes," IEEE Trans. Nucl. Sci., Vol. NS-17, December 1970, pp. 238-238.

39. Marcus, G.H., and Bruemmer, H.P., "Radiation Damage in GaAs Gunn Diodes," IEEE Trans. Nucl. Sci., Vol. NS-17, December 1970, pp. 230-232.

40. Wilson, W.E., "Neutron Irradiation Effects in LSA Oscillators," Proc. IEEE (Lett.), Vol. 59, November 1971, pp. 1683-1684.

41. Wilson, W.E., and Gregory, B.L., Neutron Induced Degradation and Failure in High Power LSA Diode Oscillators, Sandia Laboratories, SC-R-713407, October 1971.

42. Wilson, W.E., and Chaffin, R.J., "Radiation Damage Effects in Microwave Dielectric Substrate Materials," IEEE Trans. Nucl. Sci., Vol. NS-19, December 1972, pp. 82-85.

43. Klein, C.A., "Bandgap Dependence and Related Features of Radiation Ionization Energies in Semiconductors," J. Appl. Phys., Vol. 39, March 1968, pp. 2029-2038.

44. Brehm, G.E., and Pearson, G.L., "Effects of Gamma Radiation on Gunn Diodes," IEEE Trans. Electron Devices, Vol. ED-17, June 1970, pp. 475-479.

45. Wilson, W.E., Pulsed Solid-State Sources For Microwave Application, Sandia Laboratories, SC-DR-70-698, October 1970.

46. Misawa, T., "Saturation Current and Large-Signal Operation of a Read Diode," Solid State Electronics, Vol. 13, October 1970, pp. 1363-1368.

47. Borrego, J.M., Gutmann, R.J., Cottrell, P.E., and Ghandhi, S.K., "Transient Ionizing Radiation Effects on IMPATT Diode Oscillators," IEEE Trans. Nucl. Sci., Vol. NS-19, December 1972, pp. 328-334.

48. Kennedy, W.K., Jr., Eastman, L.F., and Gilbert, R.J., "LSA Operation of Large Volume Bulk GaAs Samples," IEEE Trans. Electron Devices, Vol. ED-14, September 1967, pp. 500-504.

49. Christensson, S., Woodward, D.W., and Eastmann, L.F., "High Peak-Power LSA Operation From Epitaxial GaAs," IEEE Trans. Electron Devices, Vol. ED-17, September 1970, pp. 732-738.

50. Anderson, W.A., "The Performance of a Gunn Diode Under the Influence of Gamma Radiation," Proc. IEEE (Lett.), Vol. 57, June 1969, pp. 1198-1199.

51. Chaffin, R.J., "Ionizing Radiation Effects in Microwave Cavities," IEEE Trans. Nucl. Sci., Vol. NS-18, December 1971, pp. 436-438.

52. Berg, N., and Dropkin, H., "The Effects of Ionizing Radiation on Diode Oscillators," IEEE Trans. Nucl. Sci., Vol. NS-18, December 1971, pp. 295-303.

53. Clorfeine, A.S., "Guidelines for the Design of High-Efficiency Mode Avalanche Diode Oscillators," IEEE Trans. Electron Devices, Vol. ED-18, August 1971, pp. 550-558.

54. Matsumura, M., "Computer Calculation of Silicon Avalanche Diodes," IEEE Trans. Electron Devices, Vol. ED-17, July 1970, pp. 514-519.

55. Wilson, W.E., Thermal Considerations for RF Solid-State Sources, Sandia Laboratories, SC-TM-70-175, February 1970.

56. Assour, J.M., Murr, J., Jr., and Tarangioli, D., "On the Fabrication of High-Efficiency Silicon Avalanche Diodes," RCA Review, Vol. 31, September 1970, pp. 499-516.

57. Becker, R.J., "Late Diode Entries Enliven Solid-State Source Race," Microwaves, Vol. 11, June 1972, pp. 34-48.

58. Clorfeine, A.S., "Power Dissipations Limits in Solid-State Oscillator Diodes," Microwave Journal, Vol. 11, March 1968, pp. 93-97.

59. Bravman, J.S., and Eastman, L.F., "Thermal Effects of the Operation of High Average Power Gunn Devices," IEEE Trans. Electron Devices, Vol. ED-17, September 1970, pp. 744-750.